NASA Technical Memorandum 4391

Aerothermal Test Results From the Second Flight of the Pegasus® Booster

Gregory K. Noffz, Timothy R. Moes,
Edward A. Haering, Jr., and Paul Kolodziej

OCTOBER 1992

NASA

NASA Technical Memorandum 4391

Aerothermal Test Results From the Second Flight of the Pegasus® Booster

Gregory K. Noffz, Timothy R. Moes,
and Edward A. Haering, Jr.
Dryden Flight Research Facility
Edwards, California

Paul Kolodziej
Ames Research Center
Moffett Field, California

NASA
National Aeronautics and
Space Administration
Office of Management
Scientific and Technical
Information Program
1992

CONTENTS

ABSTRACT 1

NOMENCLATURE 1

INTRODUCTION 2

TEST APPARATUS 3

INSTRUMENTATION 3

TRAJECTORY 5

DISCUSSION OF RESULTS 6
- Foil-Gauge Thermocouples 6
- Nonablating Plugs 6
- Calorimeters 6
- Differential Heating 7
- Static Pressures 7
- Orifice Protrusion 8
- Pressure-Measurement Noise 8
- Comparison With Predictions 8

CONCLUDING REMARKS 9

REFERENCES 10

ABSTRACT

A survey of temperature, heat-flux, and pressure measurements was obtained at speeds through Mach 8.0 on the second flight of the Pegasus® air-launched space booster system. All sensors were distributed on the wing-body fairing or fillet. Sensors included thin foil-gauge thermocouples installed near the surface within the thermal protection system. Thermocouples were also installed on the surface of nonablating plugs. The resulting temperature time history allowed derivation of convective heat flux. In addition, commercially available calorimeters were installed on the fillet at selected locations. Calorimeters exhibited a larger change in measured heat flux than collocated nonablating plugs in response to particular events. Similar proportional variations in heat flux across different regions of the fillet were detected by both the calorimeters and nonablating plugs. Pressure ports were installed on some nonablating plugs to explore the effects of port protrusion and high-frequency noise on pressure measurements. The effect of port protrusion on static-pressure measurements was found to decrease with increasing Mach number. High-frequency noise suppression was found to be desirable but not required on any future flight.

NOMENCLATURE

c_p	specific heat, Btu lb_m^{-1} °F^{-1}
FS	fuselage station, in.
$Heat_{abl}$	heat of ablation, Btu lb_m^{-1}
HRSI	high-temperature reusable surface insulation
k	thermal conductivity, Btu in^{-1} sec^{-1} °F^{-1} (or Btu ft^{-1} hr^{-1} °F^{-1} where specified)
L	length
LTA	Lockheed Thermal Analyzer (Lockheed Corporation, Burbank, California)
M	Mach number
NASA	National Aeronautics and Space Administration
p_{NF}	modified Newtonian flow estimate of pressure, lb ft^2
p_∞	free-stream static pressure, lb ft^{-2}
P1	pressure port at location FS = 288.4 and z = 18.25
P2	pressure port at location FS = 288.4 and z = 17.75
P3	pressure port at location FS = 253.1 and z = 18.25
P4	pressure port at location FS = 253.1 and z = 17.75
P5	pressure port at location FS = 253.1 and z = 11.25
P6	pressure port at location FS = 253.1 and z = 10.75
P7	pressure port at location FS = 241.0 and z = 11.25
P8	pressure port at location FS = 241.0 and z = 10.75
q	heat flux, Btu ft^{-2} sec^{-1}
$\bar{q}$	dynamic pressure, lb ft^{-2}
q_c	free-stream impact pressure, lb ft^{-2}
q_{conv}	convective heat flux to the surface, Btu ft^{-2} sec^{-1}

® Pegasus is a registered trademark of Orbital Sciences Corp., Fairfax, Virginia.

q_{ref}	reference surface convective heat flux, Btu ft^{-2} sec^{-1}
t	time from launch, sec
T	temperature, °F
T_{abl}	ablation temperature, °F
T_{act}	activation temperature, °F
TC	thermocouple
TPS	thermal protection system
y	lateral coordinate measured to the right from vehicle centerline, in.
z	vertical coordinate measured upward from vehicle thrust line, in.

Subscripts

abl	ablation
act	activation
inf	free stream

Greek symbols

α	angle of attack, deg
β	angle of sideslip, deg
ρ	density, lb$_m$ in^{-3}
Θ	flow incidence angle, deg
Δp	pressure difference between flush and protruding port, lb ft^{-2}
Δq	incremental difference in convective heat flux, Btu ft^{-2} sec^{-1}

INTRODUCTION

The Pegasus is an air-launched, winged rocket designed to loft small satellites into low Earth orbit. A wing and conventional tail are included on the first stage of the rocket. The resulting aerodynamic forces provide lift and control through Mach 8. The Pegasus offers the potential for performing add-on experiments, which involve installing small research packages that can be incorporated with minimal impact on the vehicle's primary orbital insertion mission. The Pegasus booster offers the advantage of being a large-scale vehicle with a large internal volume in the first stage. An additional 16 lb on the first stage reduces the orbital payload capability by only about 1 lb. Some disadvantages of the add-on concept are that the Pegasus vehicle is nonrecoverable, has ablating surfaces, and flies a predetermined trajectory designed to meet the primary payload requirements.

A series of add-on experiments has been proposed. On flights 1 and 2, the complexity of the experiments was limited to meet flight schedules. On later flights, more sophisticated experiments are planned to study phenomena such as crossflow-induced boundary-layer transition (ref. 1). The overall goal of these experiments is to perform appropriate hypersonic research, given the limitations of the Pegasus vehicle. The specific research objectives of instrumenting flights 1 and 2 were (1) to develop measurement techniques on an ablating vehicle, (2) to use these techniques to obtain in-flight temperature measurements for evaluating analytic design tools, and (3) to obtain empirical information about specific hypersonic flow features of the configuration.

The instrumentation package on the first flight consisted of foil-gauge thermocouples (TCs) and nonablating plugs distributed on the wing and wing-body fairing or fillet (sensor details are available in the next section). Heat-flux time histories derived from the nonablating plugs installed on the fillet revealed some interesting aspects of the local flow field including evidence of the wing shock interaction and flow angle effects. Details concerning flight-1 instrumentation, installation procedures, and results can be found in reference 2.

Flight-1 results from the fillet-mounted nonablating plugs were interesting enough to warrant concentrating the flight-2 instrumentation in the fillet area. The flight-2 package contained an arrangement of nonablating plugs and foil-gauge TCs similar to that on flight 1. In addition, this package was augmented with calorimeters and static pressures. The calorimeters were installed to provide a heat-flux estimate from an instrument with a cooler wall than the nonablating plugs, thus bracketing any estimate of heat flux to the unmodified surface of the fillet. Four calorimeters were placed in a row so that the wing shock would pass over each in turn yielding a better estimate of wing shock location. The location of the row was chosen based on information from flight 1. The pressure experiment investigated the effect of protruding orifices on static-pressure measurements and evaluated the need for high-frequency measurement noise suppression.

The second Pegasus mission was conducted July 17, 1991, about 15 months after the first mission. This paper presents the results of the instrumentation effort on the second flight. Temperature time histories from the foil-gauge TCs and heat-flux time histories from both nonablating plugs and calorimeters will be shown and discussed. Results of the static-pressure survey will be shown also.

The authors acknowledge the financial support of the Defense Advanced Research Projects Agency (DARPA).

TEST APPARATUS

The Pegasus is an air-launched, winged, three-stage solid rocket booster system intended to deliver payloads of up to 900 lb into low Earth orbit. Figure 1 shows the launch configuration, with a photograph of the booster mated to the B-52 carrier aircraft. The wing, tail surfaces, and wing-body fillet are all located on the first stage, as are the research instrumentation components described in this report. The expendable vehicle was approximately 49.5 ft long with a wing span of 22 ft. Total weight at launch for the flight-2 vehicle was 42,050 lb.

The wing-body fillet provides an aerodynamic junction between the wing and cylindrical rocket motor casing that forms the fuselage. The fillet structure is constructed of foam sandwiched between two 0.040-in. thick layers of graphite epoxy. The impact of sensor installation on the fillet structure will be discussed in the instrumentation section.

The wing-body fillet thermal protection system (TPS) consisted of an ablator applied over pressed cork insulation. The ablator, Thermolag T-230 (Thermal Science, Inc., St. Louis, Missouri) is a polymer substance designed to sublime around 230 °F. Cork was obtained in 0.04-in. thick pressed sheets and glued in place. Table 1 gives the thermal properties for these materials.

INSTRUMENTATION

Flight-2 instrumentation consisted of 37 channels divided among 20 TCs, 8 calorimeters, and 9 pressure measurements. Figure 2 shows the sensor distribution on the fillet. Of the 20 TCs, 12 were the foil-gauge type and were installed between the cork and ablator layers; the remaining 8 were mounted on the surface

of nonablating plugs. Foil-temperature gauges made it possible to measure temperatures between the thin layers of thermal protection with minimal perturbation. Standard TCs were installed at the surface of nonablating plugs which in turn were mounted flush with the surface of the vehicle. The plugs were fabricated from high-temperature reusable surface insulation (HRSI). HRSI, originally developed for the space shuttle, offered well-defined material properties and characteristics. Using the temperature time history at the plug surface, material properties, and geometry, the heat flux at the surface could be estimated.

Figure 3 shows a foil-gauge TCs installed within the TPS, and figure 4 shows a nonablating plug with an installation schematic. Details of the installation processes for both the foil-gauge TCs and the nonablating plugs are given in reference 2. The process for deriving a heat-flux time history from the temperature measurement on the plug surface is described in the same reference. Table 2 gives plug material properties.

On flight 2, the nonablating plugs were supplemented by eight commercially available calorimeters. Some calorimeters were collocated with plugs, and others were arranged in a row (the four sensors at fuselage station (FS) = 284.5 in fig. 2) to fine tune the estimate of shock position based on information from flight 1. Three sizes of calorimeters were installed (fig. 5). The two largest geometries (0.65 in. wide by 0.375 in. deep and 0.65 in. wide by 0.065 in. deep) were installed alongside the nonablating plugs, while the smallest calorimeters (0.187 in. by 0.375 in.) were used in the row. The calorimeters had original ranges of 0 to 3 or 5 Btu ft^{-2} sec^{-1} but all were deranged to 0 to 2 Btu ft^{-2} sec^{-1} to increase resolution.

All three calorimeters shared a common thermopile-type design, which consisted of a thin insulative wafer bonded to a metallic heat sink. A series of thermoelectric junctions was arranged so that consecutive junctions lay on opposite sides of the wafer. Heat incident on the face of the sensor was conducted through the wafer to the heat sink. The resulting differential temperature across the wafer was directly proportional to heat flux. The output signal can be made larger by increasing the number of thermoelectric junctions.

Some nonablating plugs contained pairs of static pressure ports where one port was flush with the surface and the other protruded. The protruding port was intended to simulate a static port placed on a surface that had ablated. The objective of this pressure experiment was to quantify the effect of a protruding orifice as a function of Mach number. Previous subsonic and low-supersonic research (refs. 3 and 4) has shown that the pressure measured by a protruding orifice is lower than the actual pressure.

Another issue addressed by the pressure experiment was the need for high-frequency measurement noise suppression. On future Pegasus flights it is expected that digital transducers will measure pressures. Signal aliasing can be a problem with digital measurement if the sample frequency is too low. In this experiment analog transducers were used with passive antialiasing filtering on all measurements except one to determine if there were any regions in the flight where aliasing would cause problems with a digitally measured signal.

Eight pressure ports were located on the right side of the fillet (fig. 2). Four of the nonablating plugs each contained two pressure ports. Two of the plugs included protruding orifices. Figure 6 shows a diagram of a plug with orifices installed. Pressure port P6 had a 0.05-in. protruding tube and pressure port P8 had a 0.10-in. protruding tube. The exposed pressure tubing was quartz glass (0.125-in. inside diameter, 0.175-in. outside diameter) which extended through the plug. Internally, this was connected to high-temperature silicon tubing (0.156-in. inside diameter) which extended from the glass tubing to the transducer box.

Figure 7 shows a schematic of the pressure measurement system. Differential pressure transducers measured the surface pressures relative to a reference pressure manifold (volume = 0.75 in^3). The reference pressure was measured by an absolute pressure transducer. The absolute transducer was ranged from 0 to 30 lb in^2 with a measurement accuracy of 0.005 lb in^2 and 20-bit resolution. The differential transducers were ranged from ± 1 lb in^2 for ports P1 and P2 and from -1.5 to 0.5 lb in^2 for ports P3 through P8.

The measurement accuracy of the differential measurements was 0.008 lb in^2 and an 8-bit word was used which gave a resolution of 0.008 lb in^2. Combining the absolute measurement accuracy and the differential measurement accuracy gave a laboratory calibration root-mean-square accuracy of 0.012 lb in^2 (1.73 lb ft^2).

The transducers also were calibrated on the vehicle with the instrumentation system powered up. With few exceptions, the calibrations fell within the 1.73 lb ft^2 accuracy. On flight day, preflight zeros were obtained to determine any zero shifts in the calibrations. No significant zero shifts were expected since these transducers were calibrated only 6 days before the flight. However, significant zero shifts were discovered. The zero shifts for ports P1 through P8, respectively, were 20.2, 18.7, 5.9, 8.4, 10.8, 4.3, 6.8, and 4.8 lb ft^2. These shifts were subtracted from the flight data. It is also possible that a slope change could have occurred in the calibration; however, there was no way to determine this from the preflight data.

The absolute pressure transducer was a digital sensor while the differential pressures were measured using analog transducers. A passive antialiasing filter circuit was applied to the differential pressure measurements (except P6). This first-order filter was designed to roll off the signal at 10 Hz. The transducers were wrapped in insulating blankets to prevent rapid temperature changes and hence calibration inaccuracies. TCs were used to monitor the transducer temperatures throughout the flight. The flight data showed that the differential transducers were a constant 75 °F throughout the flight and that the absolute transducer was at a constant 42 °F. All transducer calibrations were valid at these temperatures.

Pressure port P1 was connected to the reference pressure manifold as well as to a differential pressure transducer. This port was chosen to supply the reference pressure since its location on the fillet gave it a 5° incidence to the free stream with no sideslip. Pressure ports P3 through P8 were at 0° incidence to the free stream with no sideslip. At any point in the flight, port P1 (as well as port P2) was expected to measure the highest pressure on the fillet because of its 5° inclination. The pressure at port P1 was estimated in preflight analysis using Newtonian flow techniques (ref. 5). From the estimated pressures the required differential transducer ranges were then determined. The 124 in. of tubing from the surface of port P1 to the reference pressure manifold slightly lagged the reference pressure and damped out any higher frequency pressure fluctuations.

TRAJECTORY

No onboard airdata measurements were taken on the Pegasus. Free-stream airdata quantities were estimated postflight by a combination of data from an onboard inertial navigation system, information from three ground-based radar tracking sites, and atmospheric data from balloons, stratospheric charts, and climatological information. Reference 2 contained a detailed account of airdata estimation on flight 1, which by comparison had access to eight ground-based radars.

Figures 8(a) and 8(b) show flight condition parameters from launch to first-stage separation. The Pegasus began its path to orbit under the right wing of the NASA B-52. Launched from about 42,000 ft, the Pegasus dropped away from the bomber for approximately 5 sec before the first stage ignited. A 2-g pullup was then executed, during which the vehicle reached a maximum angle of attack of about 22°. Angle of attack was reduced to about 3° from about Mach 2.5 to 3.5. Angle of attack was near 0° for the remainder of first-stage flight. Maximum dynamic pressure was about 820 lb ft^2 and occurred 30 sec after launch. At that time, altitude was just under 60,000 ft and Mach number was about 2.5. In comparison to flight 1, the flight-2 vehicle returned to a lower angle of attack (about 3°) after the initial pitch up.

DISCUSSION OF RESULTS

Foil-Gauge Thermocouples

Figure 9 shows temperature time histories measured by the foil-gauge TCs at the ablator-insulator interface. Initially, temperatures are around −20 °F and begin to rise about 10 sec after launch. Of the 12 channels, 7 reached the maximum range of 320 °F. Shown in figures 9(a) through 9(e) are temperature time histories for each row of TCs at various fuselage stations. At each station, TCs closer to the wing underside experience both higher rise rates and higher ultimate temperatures. The only exceptions are the TCs at the farthest aft fuselage station (FS = 241.0, fig. 9(e)), with the TC at $z = 8.5$. The data from this sensor before $t = 8$ sec are unrealistic and inconsistent with other results. They are shown only for the sake of completeness.

Nonablating Plugs

Figure 10 is a typical temperature time history measured at the surface of a nonablating plug (FS = 288.4, $z = 18.0$). At launch, the plug surface is about −40 °F and the temperature begins to rise about 6 sec after launch. A maximum of about 575 °F is attained about 59 sec after launch, followed by a sharp change in slope. The plugs attain a higher surface temperature than the surrounding ablator because comparatively little heat is conducted into them and no energy is dissipated with ablation products.

Figures 11(a) through 11(f) depict convective heat transfer (q_{conv}, which is equal to the sum of the radiation and conductive components) time histories derived from the plug surface temperatures using Lockheed Thermal Analyzer (LTA) program (Lockheed Report 18902, *Thermal Analyzer Computer Program for the solution of General Heat Transfer Problems*). For details concerning plug heat-flux derivation, see reference 2. Peak values range from about 1.0 to 1.5 Btu ft^{-2} sec^{-1}. All maximum values occur between 50 and 60 sec. The absolute value of convective heat flux to the plug surface is lower than the heat flux to the surrounding TPS because the plug surface temperature is higher and results in a lower difference between surface and recovery temperatures. As shown below, the heat fluxes measured by the calorimeters are much higher than for the nonablating plugs because the metallic construction of the calorimeters conducts heat away from the surface more readily. The resulting lower wall temperature provides a larger temperature difference and thus a larger heat flux.

Calorimeters

Based on data from the nonablating plugs flown on flight 1, the calorimeters were ranged to a maximum of 2 Btu ft^{-2} sec^{-1}. Unfortunately, because of the comparatively cool wall discussed above and the higher sustained dynamic pressure trajectory of flight 2, all but one of the calorimeters exceeded their maximum range. Maximum heat flux ranges varied from channel to channel because of variations in scale factors and full-scale outputs among the individual sensors.

Figure 12 shows the heat-flux time histories from the calorimeters. All calorimeters experience a momentary decrease in heat flux between 25 and 30 sec after launch. This coincides with the aircraft pitch down from $\alpha = 18°$ and a change in sideslip from $\beta = +7°$ to 0°. This effect is also visible in most of the nonablating plugs but is not nearly as well defined. The effect seems strongest in sensors ranging from the upper right to the lower left on the fairing. Comparing the nonablating plug/calorimeter side-by-side installations at FS = 280.6, $z = 11.0$ and at FS = 253.1, $z = 23.0$ (figs. 13(a) and 13(b)), the event between 25 and 30 sec is more pronounced for the calorimeters than for the nonablating plugs. The calorimeters are more sensitive than the plugs in the sense that a given event elicits a larger change in heat flux.

Differential Heating

The heat-flux data from the nonablating plugs and the calorimeters may be interpreted with respect to the trajectory and sensor location. By using supersonic wedge tables (ref. 6) for several trajectory flight conditions, an estimate was made of the wing leading-edge shock-wave position, superimposed on the sidewall of the fairing (fig. 14(a)). This estimate does not account for offsets caused by the 1-in. wing leading-edge radius or fuselage bow shock effects. Based on this estimate, however, the sensors on the forward corner of the fairing, farthest from the wing, are expected to be upstream of the wing shock for flight conditions in which aerodynamic heating is significant. When compared, heat-flux time histories from the two nonablating plugs in this area agree favorably throughout the flight profile (fig. 11(a)). Therefore, an average of the data from these two sensors (fig. 14(b)) will be referred to as the reference heating, q_{ref}, and used to normalize data from other nonablating plugs.

Differential heating Δq is defined as

$$\Delta q = q_{conv} - q_{ref}$$

and is shown for the remaining nonablating plugs in figure 15. No appreciable additional heating is apparent for the sensors closest to the lower surface of the wing (figs. 15(a), (b), and (e)) at elevated angle of attack ($t < 30$ sec). This differs from results seen on the first flight. The difference may be because the flight-2 vehicle pitched down before it experienced significant aerodynamic heating. Between $t = 30$ and 60 sec, differential heating in the wing shock region (figs. 15(a), (d), and (f)) climbs to a maximum between 53 and 55 sec. The sensor farthest aft and farthest from the wing (fig. 15(f)) experiences the most severe differential heating of $\Delta q = 0.6$ Btu ft^{-2} sec^{-1}. At this time, the reference heating, q_{ref}, is about 0.83 Btu ft^{-2} sec^{-1}, thus the sensor depicted in figure 15(f) is experiencing about 1.7 times the reference heating.

Figure 16 shows the calorimeter reference heating, which is the average of the time histories found in figure 12(e). The sensors that comprise the reference heating are located forward and away from the wing, as in the case of the nonablating plugs. Calorimeter differential heating, described below, is defined in the same manner as differential heating on the nonablating plugs.

Figures 17(a) through 17(e) show differential heating data for the calorimeters located away from the reference region. Differential heating data are not shown when either the sensor or the reference heating is off scale. Figure 17(a) shows differential heating for the calorimeter at FS = 288.4, $z = 23.0$. Maximum observed Δq for this sensor is about 0.9 Btu ft^{-2} sec^{-1}, or about twice the reference heating and occurs between 65 and 70 sec after launch. Even higher differential heating of about 1.4 Btu ft^{-2} sec^{-1} is observed for the sensor at FS = 284.5, $z = 22.0$ (fig. 15(c)). The sensors located just above and below (figs. 17(b) and 17(d), respectively) each experience a negative differential heating during the same period. This inconsistency is not understood at this time and will require further investigation. The sensor depicted in figure 17(e) exhibits differential heating similar to the nearby nonablating plug (fig. 15(b)) from $t = 65$ sec to the end of the first-stage flight. The differential heating analysis for the calorimeters was greatly hampered by the range limit problem.

Static Pressures

Figure 18 shows time histories of the absolute and differential pressure measurements. Approximately 16 sec after launch, pressure ports P3 through P8 exceeded the pressure range of the transducers during an unplanned $-11°$ sideslip excursion. About 58 sec after launch (Mach 4.8 and 96,000 ft altitude), the differential pressure measurements began drifting unexpectedly. The fact that something was wrong became obvious as adding the differential pressure measurement to the reference pressure caused negative

absolute pressures for ports P1, P3, P4, and P6. The same type of transducer was subsequently tested in an altitude chamber at NASA Dryden. This drifting phenomenon was repeated for altitudes greater than 70,000 ft. It is hypothesized that as the ambient air became less dense, the heat generated within the transducer was no longer easily dissipated. Consequently, the temperature of the transducer's sensing element increased and caused the output to be erroneous for the remainder of the flight.

Orifice Protrusion

In this experiment, pressure port P6 protruded 0.05 in. above the surface and pressure port P8 protruded 0.10 in. above the surface. To determine the protrusion effect, measurements from flush orifices (P5, P7) were compared to measurements from adjacent protruding orifices (P6 and P8, respectively). Figure 19 shows the error, Δp, normalized by dynamic pressure. At low Mach numbers, the magnitude of the error is in very good agreement with results from references 3 and 4. As Mach number increased, the error decreased to about 0.02 at Mach 5. Unfortunately, the information at higher Mach numbers is not available.

Pressure-Measurement Noise

The effect of high-frequency noise suppression was also studied in the pressure experiment. Figure 18(d) shows pressure port P5 with noise suppression and pressure port P6 without noise suppression. As shown, a considerably noisier signal was obtained from port P6. The magnitude of the noise is fairly constant throughout the flight. In postflight analysis, the measurement from port P6 was run through a 1-Hz low-pass filter. This induced a 0.225-sec lag on the filtered measurement. Correcting for this lag, the filtered P6 measurement is compared with the unfiltered measurement in figure 20. Although the unfiltered signal is noisy, the signal-to-noise ratio is still large enough to obtain an accurate pressure measurement. In this flight, therefore, there was no region where antialiasing was required to obtain the pressure measurement. It is possible that aliasing could still be a problem on future flights using different pressure measurement locations and different pressure-line geometries. However, this experiment showed no evidence of potential problems.

Comparison With Predictions

A simple prediction can be obtained for the forward facing pressure ports P1 and P2 (FS = 288.9) using modified Newtonian flow. The plug containing these ports is located on the fillet so that the incidence to the free stream is 5° at 0° sideslip. The modified Newtonian flow estimate for the pressure is

$$p_{NF} = q_c \cos^2\Theta + p_\infty$$

where

$$\cos\Theta = (\cos 85°)(\cos\beta)(\cos\alpha) + (\sin 85°)(\sin\beta)$$

Figure 21 shows a comparison between the measured pressure at port P1 and the Newtonian flow estimated pressure. As expected, the solutions converge as Mach number increases (ref. 5).

CONCLUDING REMARKS

Temperature, heat flux, and pressure measurements from the second flight of the Pegasus air-launched booster were obtained on the ablating surface of the wing-body fillet. Temperature measurements were obtained within a thin-layered, ablating thermal protection system and on the surface of small nonablating plugs mounted flush on the fillet. Heat-flux time histories were derived from the plug surface temperature measurements. Commercially available calorimeters that provide heat-flux time histories were also installed on the wing-body fillet, in some cases adjacent to a nonablating plug. This data can help to evaluate the effectiveness of the aerothermal design tools used in developing the Pegasus vehicle and to provide empirical information related to specific hypersonic flow features of the configuration.

Temperatures measured within the fairing thermal protection system often exceeded the data range limit of 320 °F. Sensors located near the wing lower surface tended to reach higher temperatures than sensors at the same fuselage station but farther from the wing. This phenomenon probably resulted from increased compression in the wing flow field.

Derivations of convective heat flux from the nonablating plugs produced consistent time histories for those sensors forward of the predicted wing leading edge shock position. The maximum heating rate measured near the shock was about 1.7 times the value measured ahead of the shock. Data from sensors aft of the shock were difficult to correlate with changes in angle of attack, because the vehicle pitched down to minimal angle of attack ($< 4°$) before significant aerodynamic heating took place.

All but one of the commercially available calorimeters experienced heat fluxes in excess of the data range limit (approximately 2 Btu ft^{-2} sec^{-1}) during significant portions of the flight. This limited the amount of postflight analysis possible with the calorimeter data when compared with the data from the nonablating plugs. Comparing collocated calorimeters and nonablating plugs, both showed similar percentage changes in heat flux caused by a given event.

As with the plugs, the calorimeters located in the region ahead of the wing shock interaction measured roughly similar heat-flux time histories. Meanwhile, calorimeters in the shock region experienced up to twice as much heating.

The pressure-measurement experiment showed good results for the flight below Mach 4.8. An interesting instrumentation problem was discovered in the pressure-measurement experiment. As altitude increased beyond 96,000 ft, it is believed that the differential transducers could no longer dissipate internally generated heat. This caused the differential transducer measurements to be useless after 96,000 ft. For future Pegasus missions, it will be necessary to verify with ground tests the performance of pressure transducers in a high-altitude (low ambient pressure) environment.

The adverse effect of orifice protrusion from the surface was demonstrated at two locations on the fillet. The adverse effect diminished as Mach number increased. High-frequency noise suppression in the pressure transducer measurement was determined to be desirable but not required. Consequently, digital pressure transducers can be used effectively to measure pressures on the Pegasus vehicle.

REFERENCES

1. Bertilrud, Arild, Paul Kolodziej, Greg Noffz, and Afal Godil, "Plans for In-Flight Measurement of Hypersonic Crossflow Transition on the Pegasus Launch Vehicle," AIAA-92-4104, Aug. 1992.

2. Noffz, Gregory K., Robert E. Curry, Edward A. Haering, Jr., and Paul Kolodziej, *Aerothermal Test Results From the First Flight of the Pegasus Air-Launched Space Booster*, NASA TM-4330, 1991.

3. Gracey, William, *Measurement of Aircraft Speed and Altitude*, NASA RP-1046, 1980.

4. Moes, Timothy R. and Robert R. Meyer, Jr., *In-Flight Investigation of Shuttle Tile Pressure Orifice Installations*, NASA TM-4219, 1990.

5. Anderson, John D., Jr., *Hypersonic and High Temperature Gas Dynamics*, McGraw-Hill Book Company, 1989.

6. Ames Research Staff, "Equations, Tables and Charts for Compressible Flow," *Thirty-Ninth Annual Report of the National Advisory Committee for Aeronautics*, NACA Report 1135, 1953, pp. 613–681.

Table 1. Properties of TPS materials.

Material	ρ, $lb_m\ in^{-3}$	k, Btu $in^{-1}\ sec^{-1}\ °F^{-1}$	c_p, Btu $lb_m^{-1}\ °F^{-1}$	$Heat_{abl}$, Btu lb_m^{-1}	T_{abl}, °F	Description
Cork	0.0177	0.925×10^{-6}	0.47	n/a	n/a	Multipurpose insulator. Organic fiber. Bonded in place.
Thermolag	0.0521	1.85×10^{-6}	0.3	750	230	Low-temperature ablative material. Polymer. Spray-on application.

Table 2. HRSI material properties; HRSI density (LI-2200) = 22 $lb_m\ ft^{-3}$.

(a) Thermal conductivity (Btu $ft^{-1}\ hr^{-1}\ °F^{-1}$).

	Pressure, atmosphere					
Temperature, °F	10^{-5}	10^{-4}	10^{-3}	10^{-2}	10^{-1}	1
−250	0.0133	0.0133	0.0167	0.0267	0.0300	0.0333
−150	0.0150	0.0150	0.0183	0.0283	0.0333	0.0367
75	0.0183	0.0183	0.0233	0.0333	0.0408	0.0467
500	0.0250	0.0250	0.0317	0.0408	0.0558	0.0650
1000	0.0358	0.0358	0.0442	0.0533	0.0783	0.0900
1500	0.0500	0.0500	0.0600	0.0708	0.1058	0.1192
1700	0.0583	0.0583	0.0683	0.0808	0.1192	0.1342
2000	0.0692	0.0692	0.0833	0.0983	0.1417	0.1583
2300	0.0842	0.0842	0.1000	0.1200	0.1658	0.1883

(b) Specific heat.

Temperature, °F	c_p, Btu $lb_m^{-1}\ °F^{-1}$
−250	0.070
−150	0.105
0	0.150
250	0.210
500	0.252
750	0.275
1000	0.288
1250	0.296
1500	0.300
1700	0.302
1750	0.303
3000	0.303

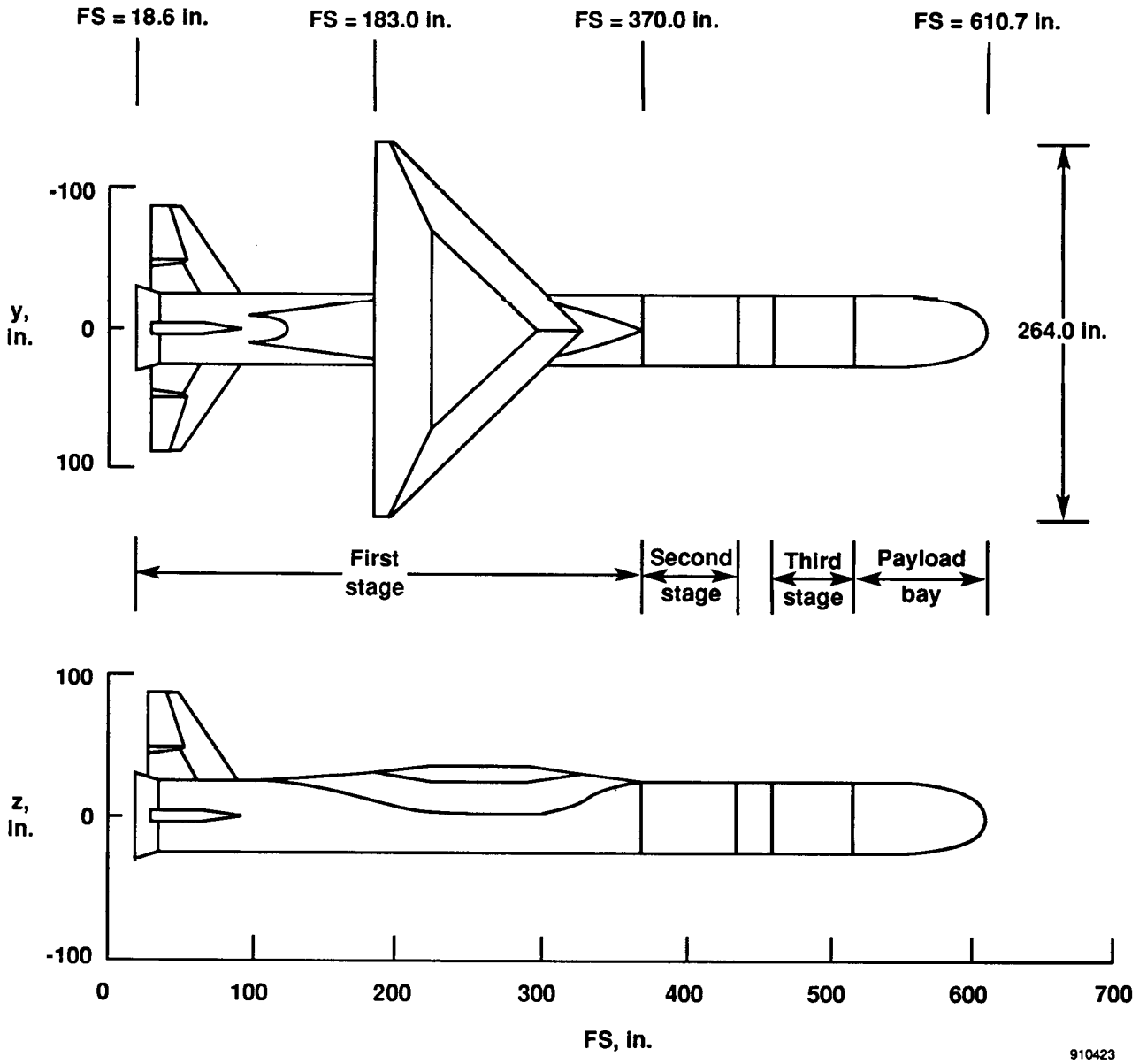

(a) Pegasus two-view.

Figure 1. Pegasus launch configuration.

EC 91-348-3

(b) B-52 carrier aircraft and Pegasus.

Figure 1. Concluded.

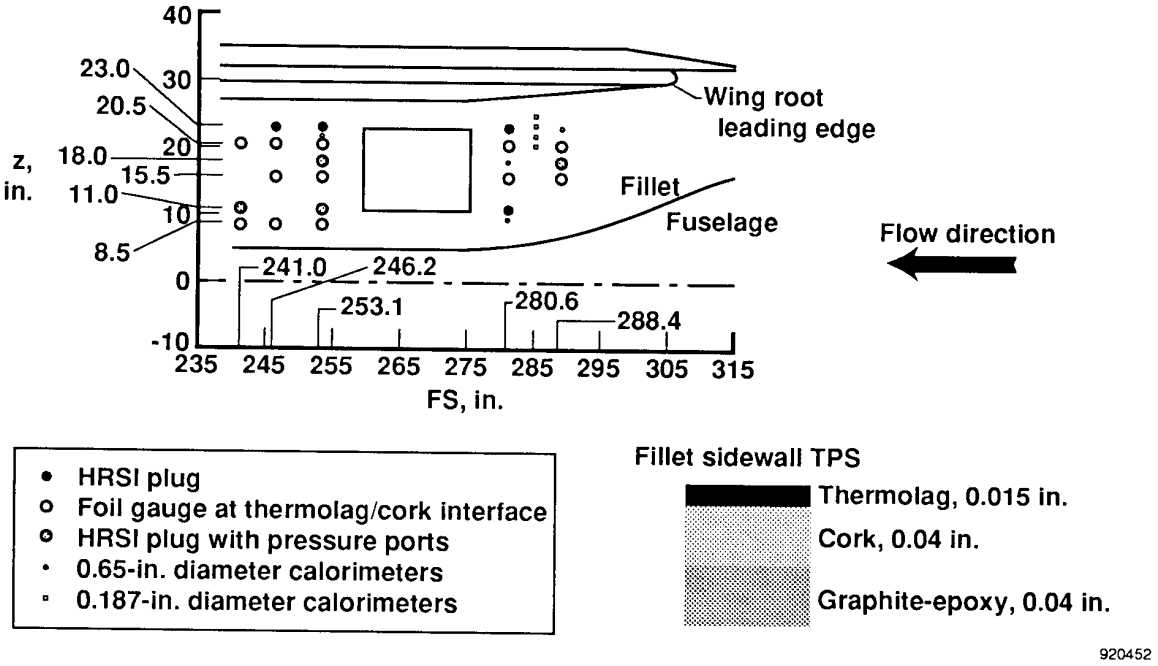

Figure 2. Flight-2 instrumentation layout.

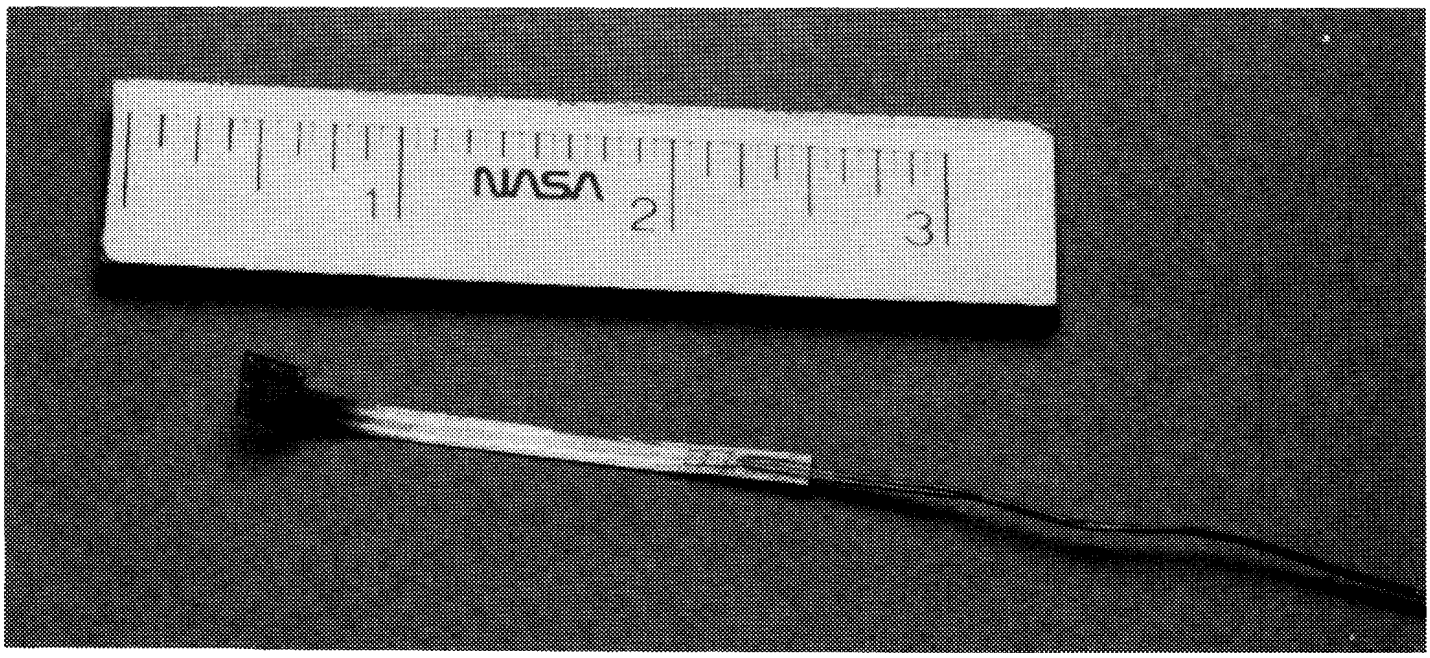

EC 89-317-005

Figure 3. Foil TC sensor and leads.

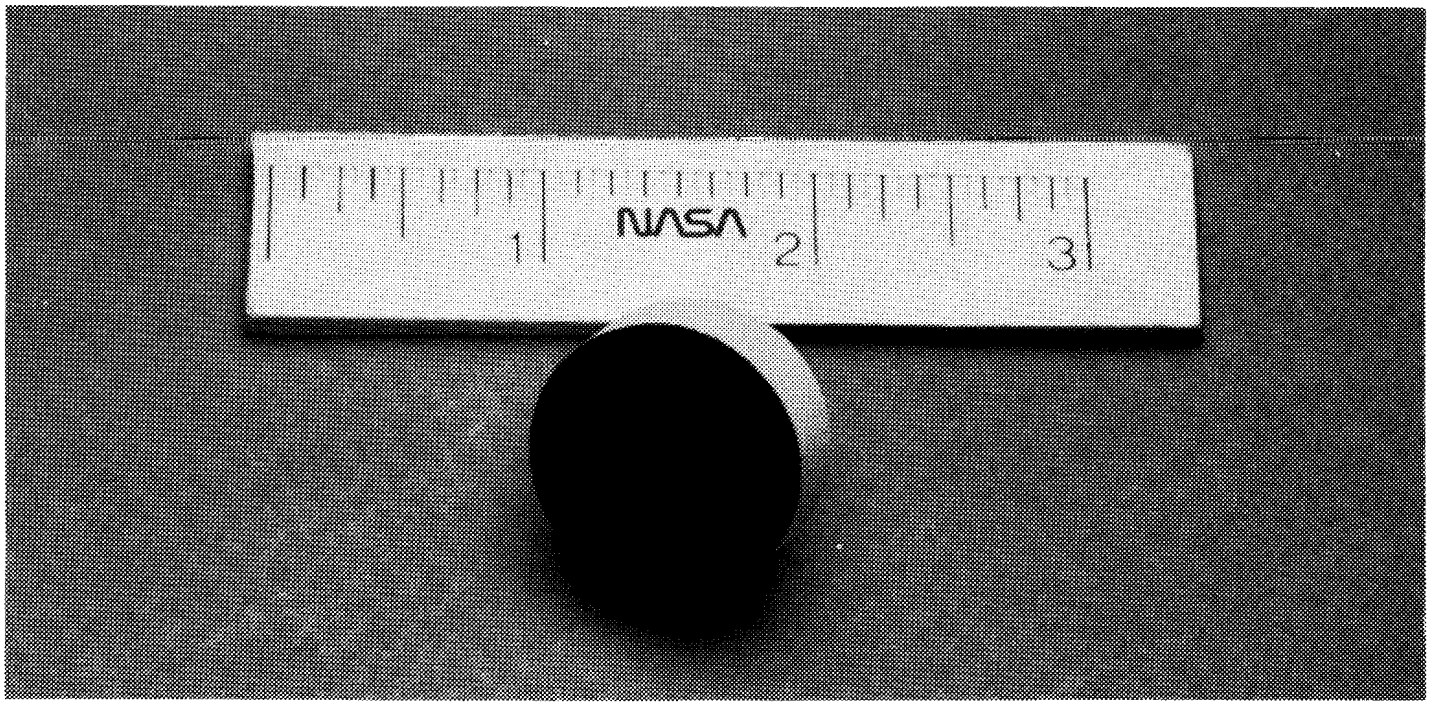

EC 89-317-003

(a) HRSI plug.

Figure 4. HRSI plug illustrations.

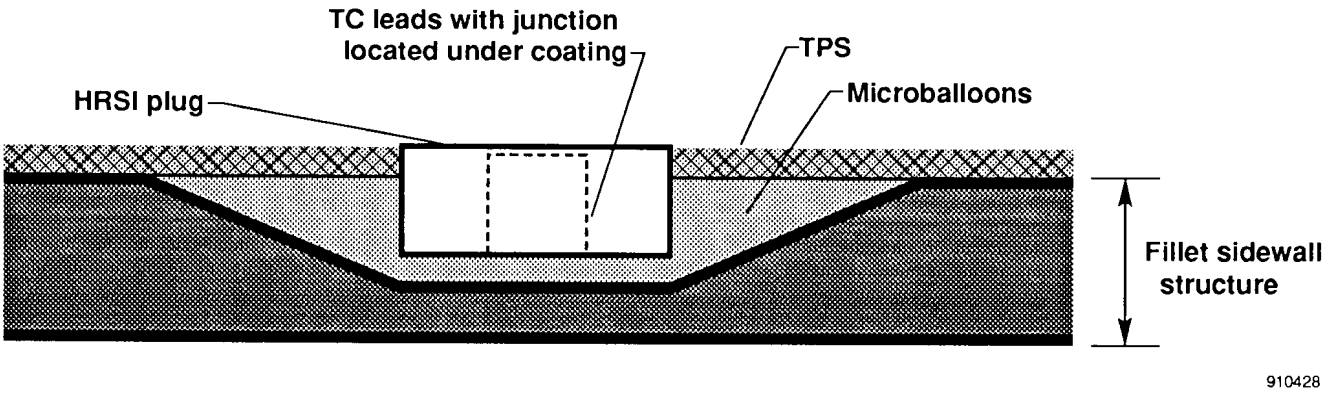

(b) Cross-sectional diagram of HRSI plug installation.

Figure 4. Concluded.

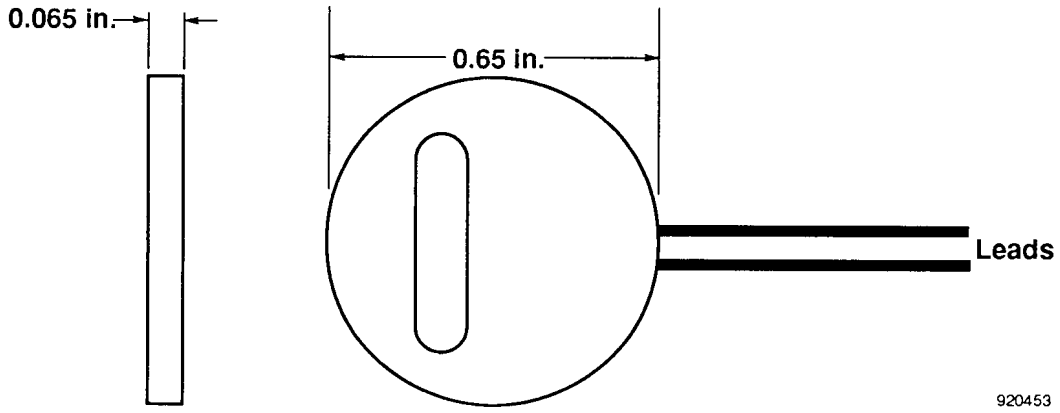

(a) 0.65 by 0.065 in. calorimeters located at FS = 280.6, z = 11.0 and at FS = 253.1, z = 23.0.

Figure 5. Calorimeter geometries.

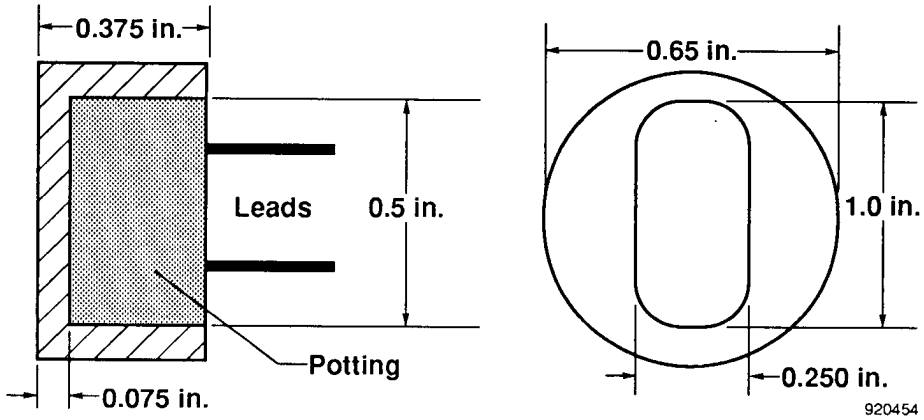

(b) 0.65 by 0.375 in. calorimeters located at FS = 288.4, z = 23.0 and at FS = 280.6, z = 18.0.

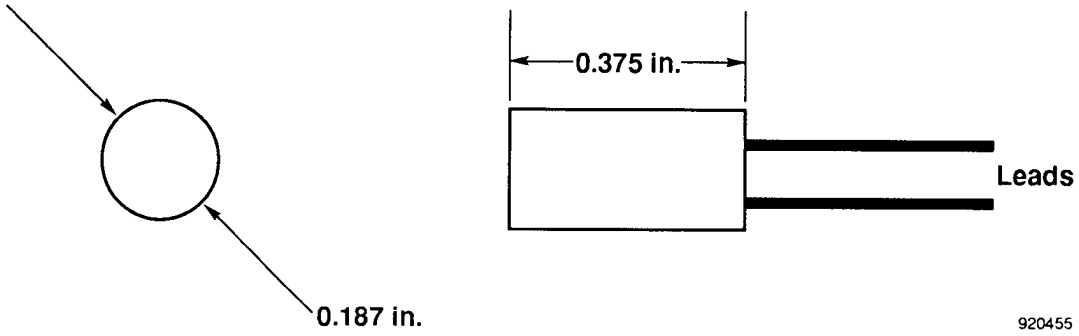

(c) 0.187 by 0.395 in. calorimeters located at FS = 284.

Figure 5. Concluded.

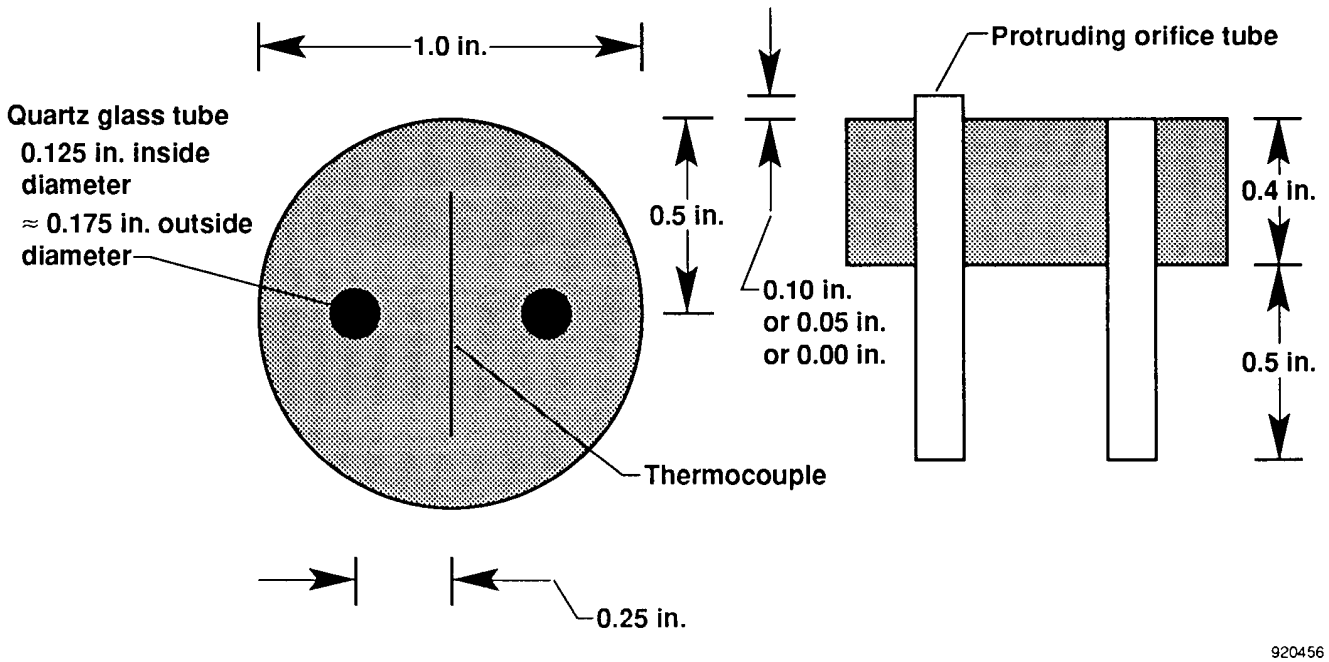

Figure 6. Pegasus pressure orifice plugs.

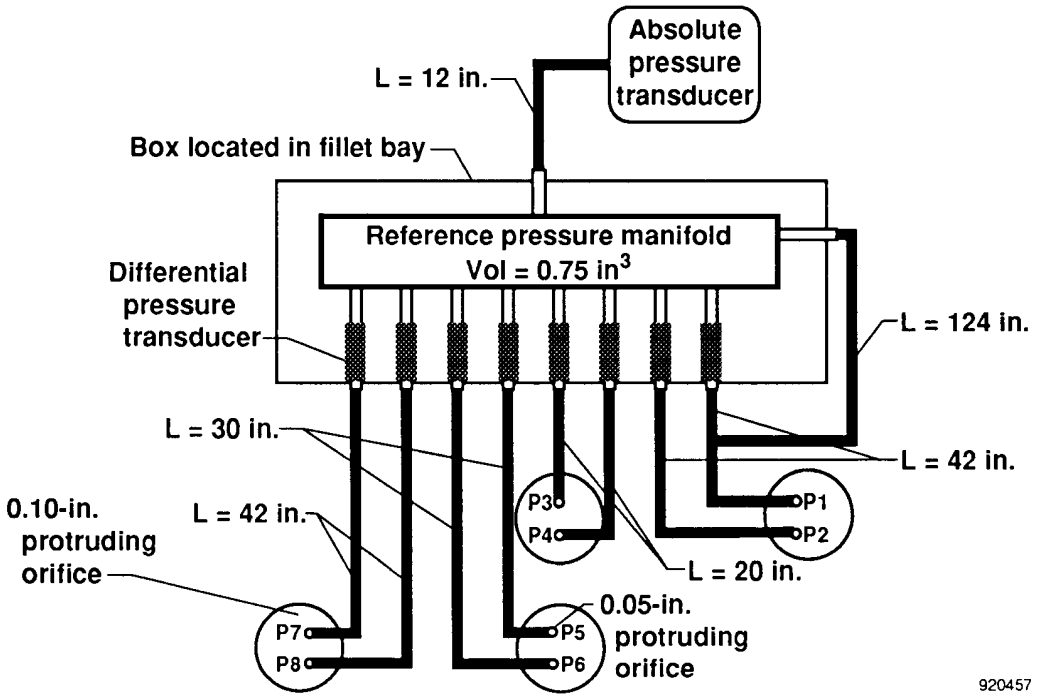

Figure 7. Pressure experiment hardware arrangement.

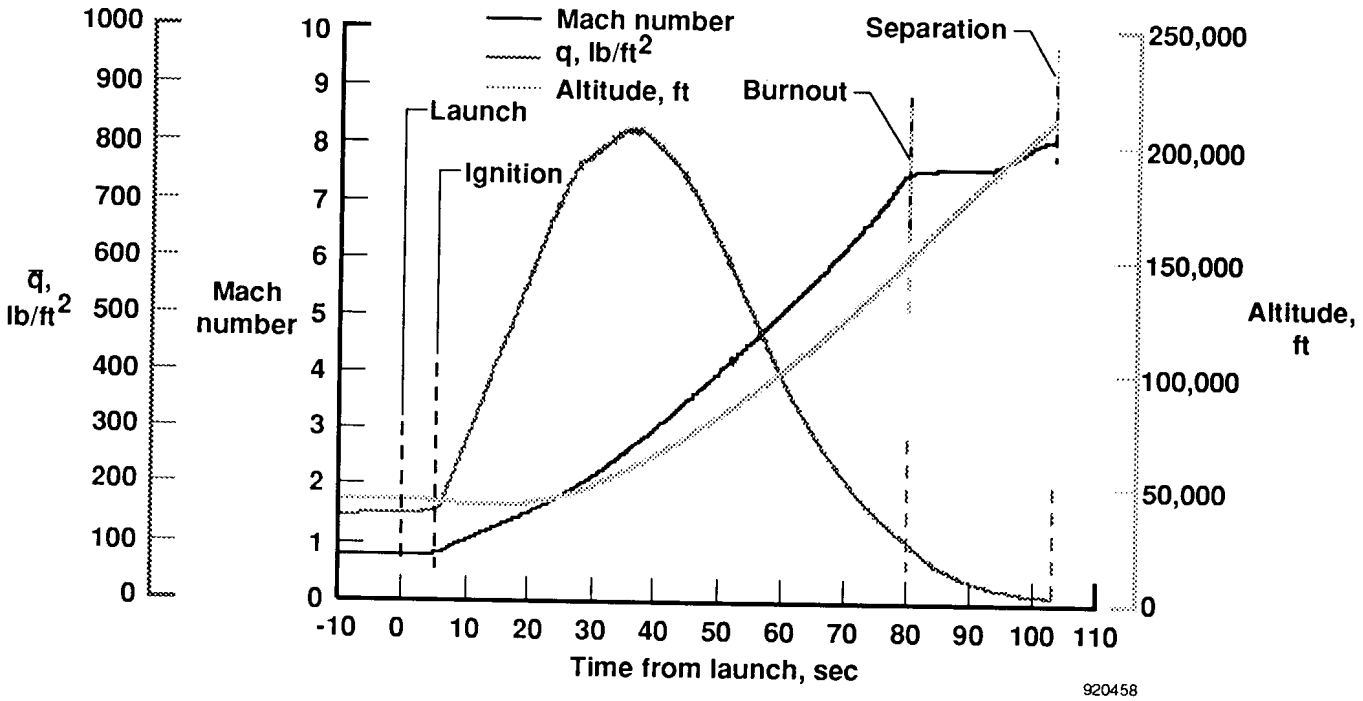

(a) Mach number, dynamic pressure, and altitude.

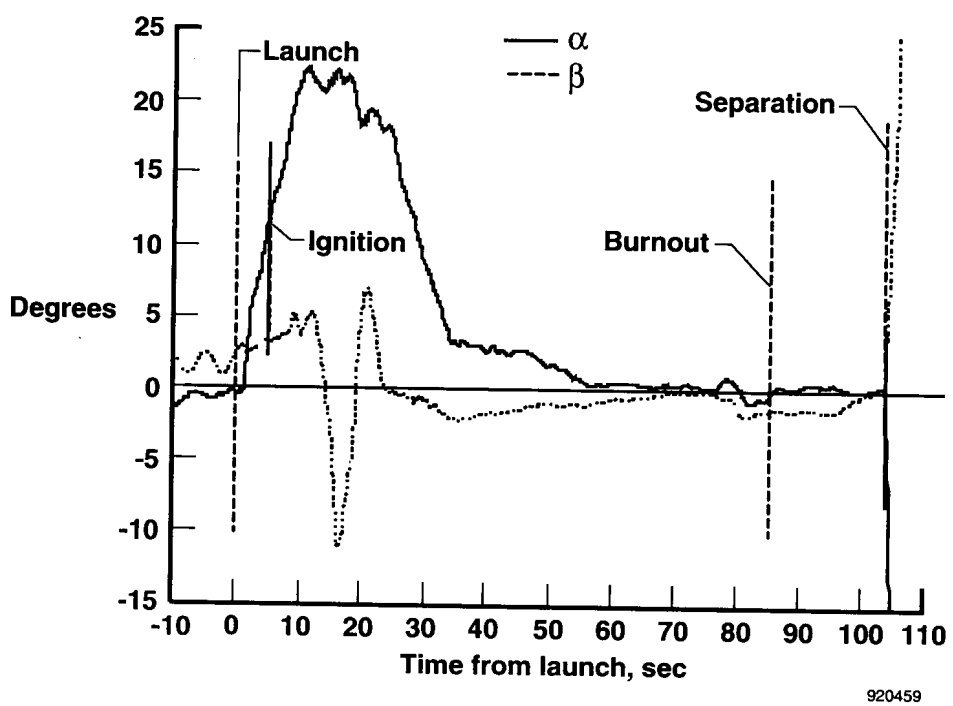

(b) Angles of attack and sideslip.

Figure 8. Trajectory parameters.

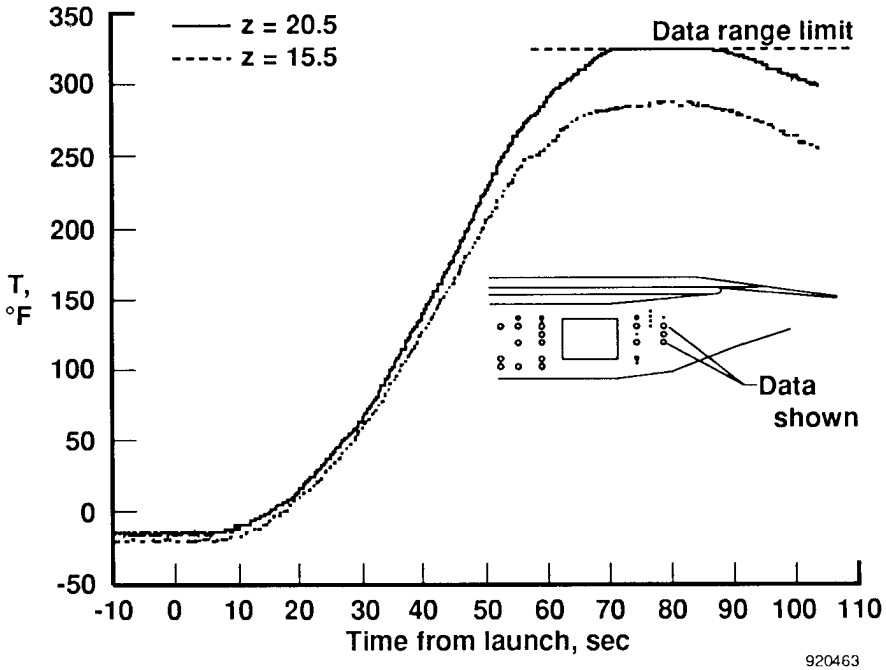

(a) FS = 288.4.

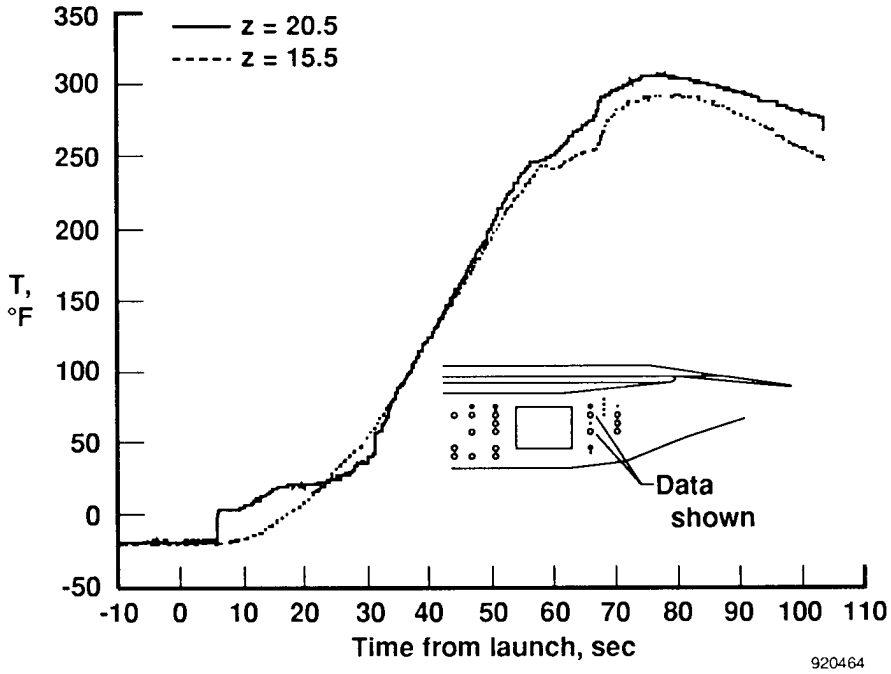

(b) FS = 280.6.

Figure 9. Fillet temperatures, thermolag-insulator interface.

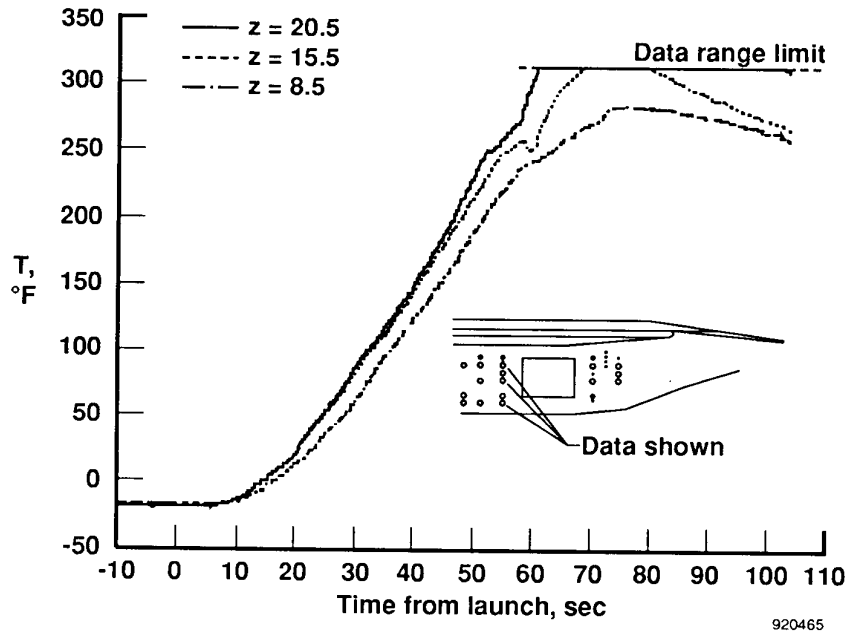

(c) FS = 253.1.

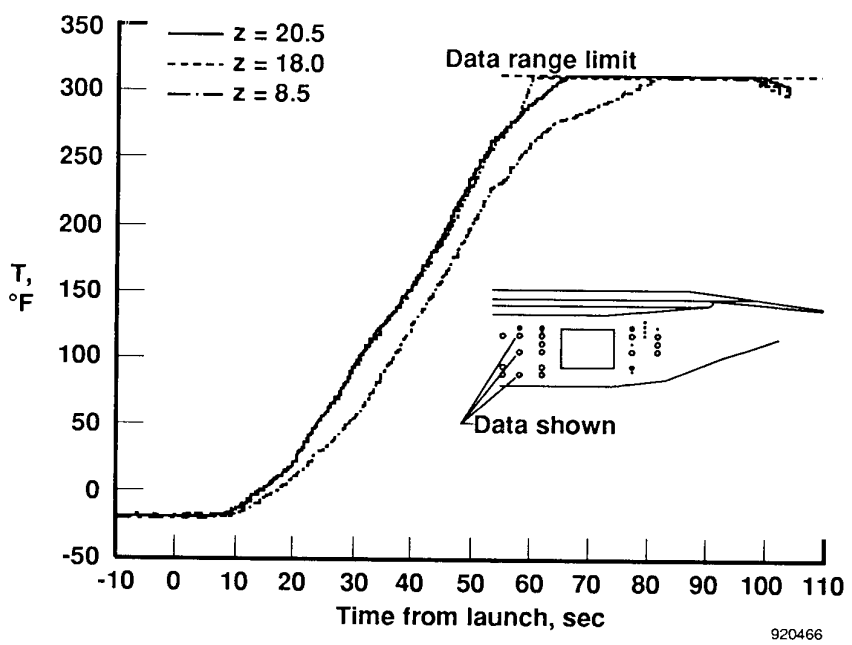

(d) FS = 246.2.

Figure 9. Continued.

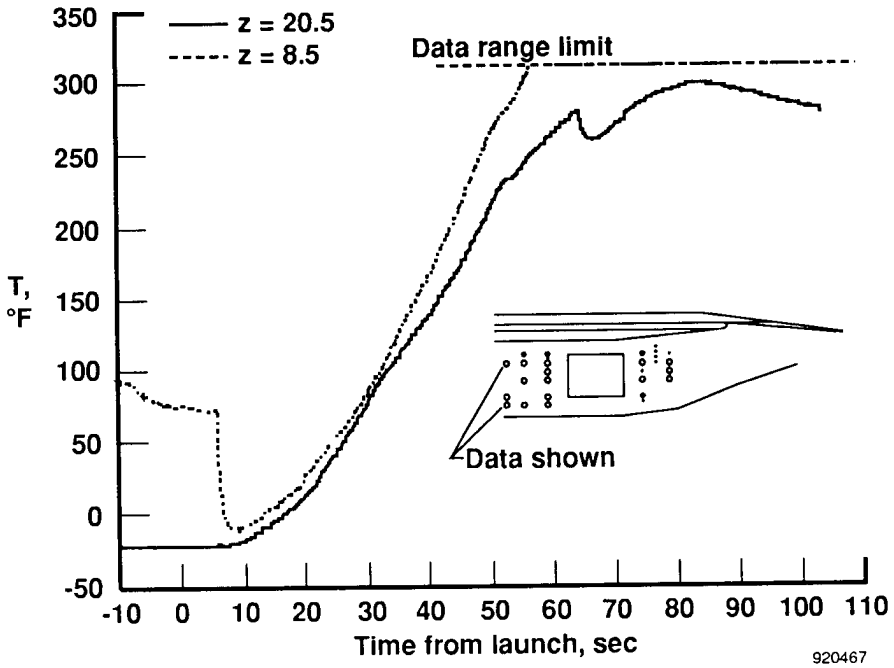

(e) FS = 241.0.

Figure 9. Concluded.

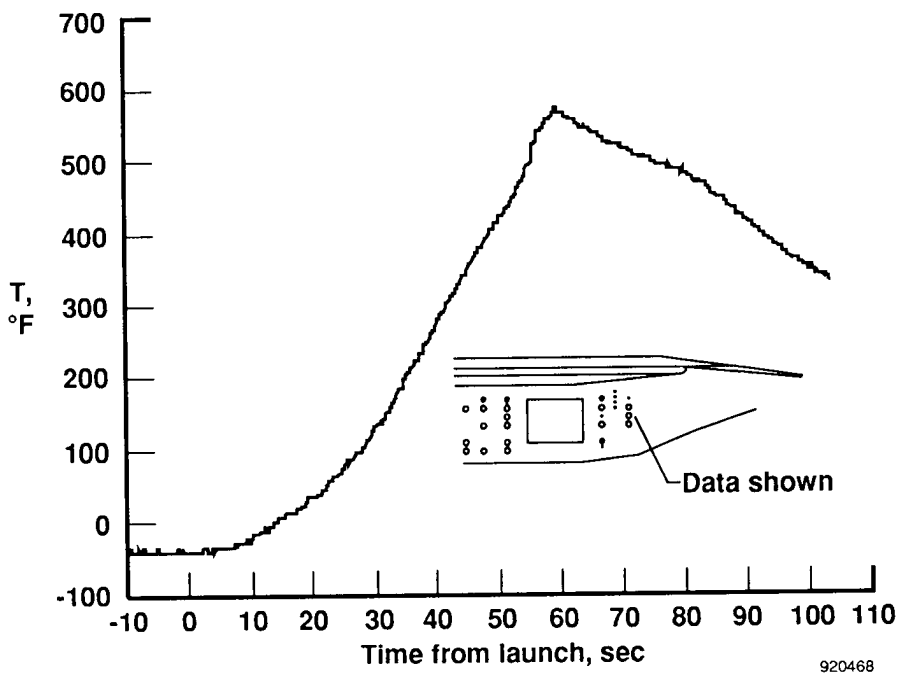

Figure 10. Temperature time history at a plug surface (FS = 288.4, z = 18.0).

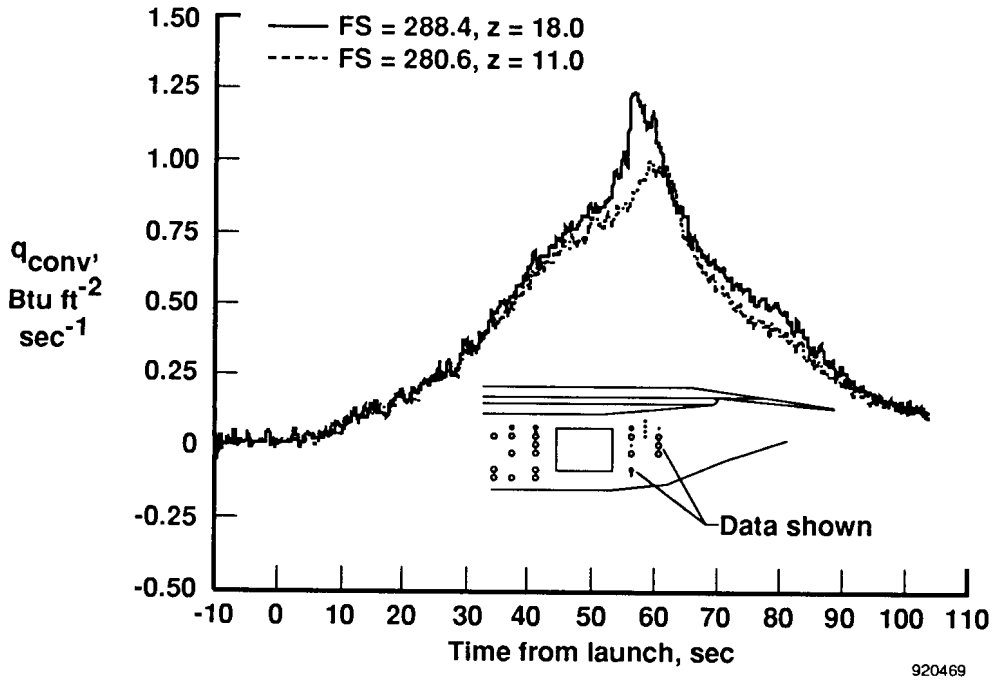

(a) FS = 288.4, z = 18.0 and FS = 280.6, z = 11.0.

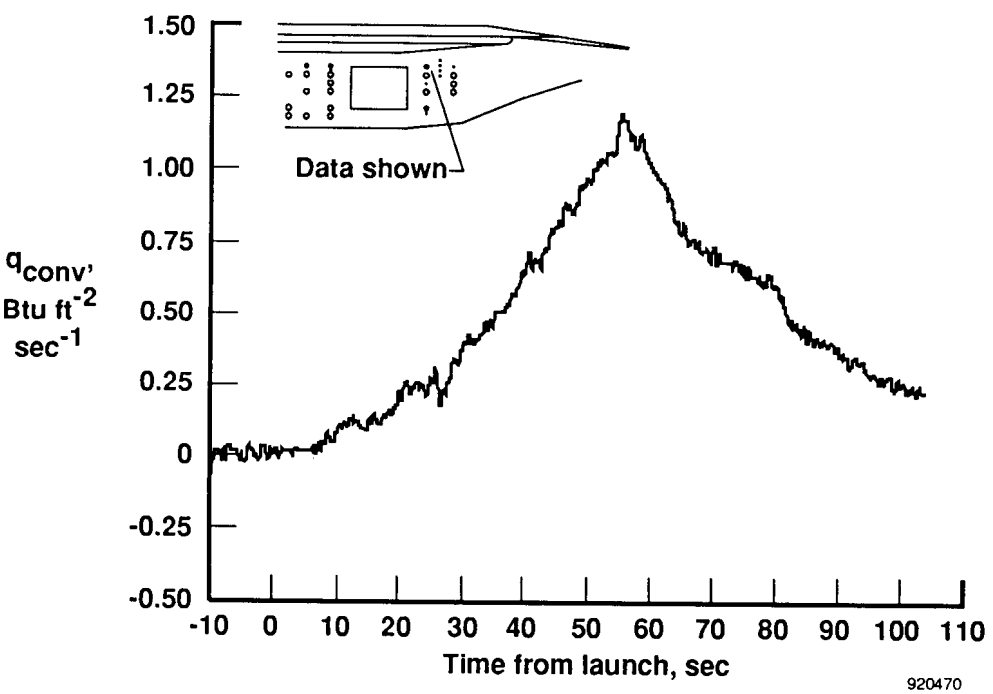

(b) FS = 280.6, z = 23.

Figure 11. Derived heat-flux estimates on nonablating plugs.

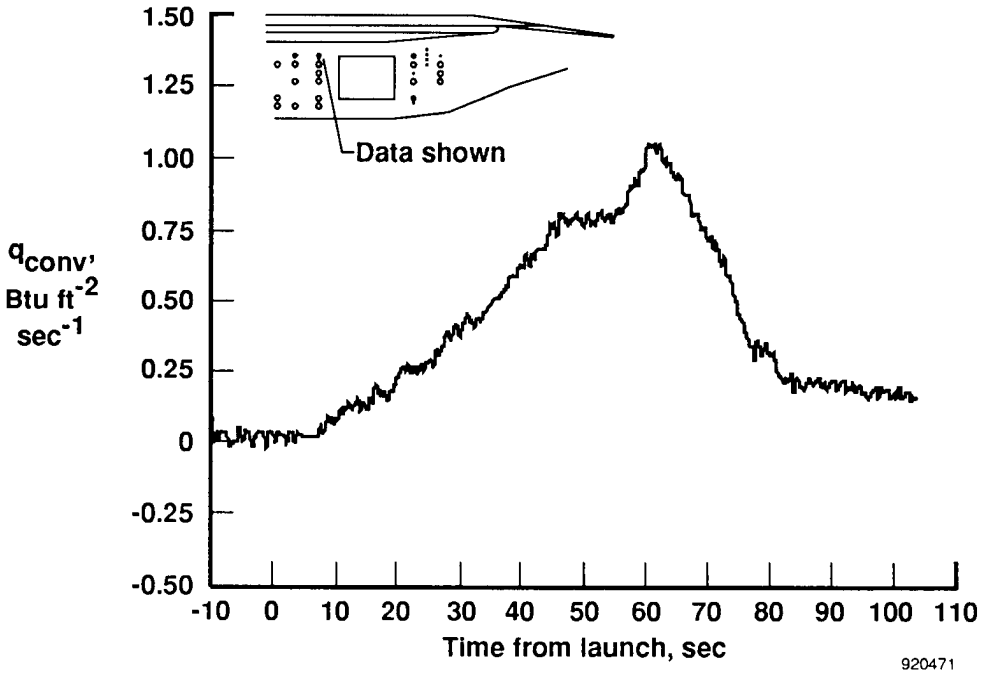

(c) FS = 253.1, z = 23.0.

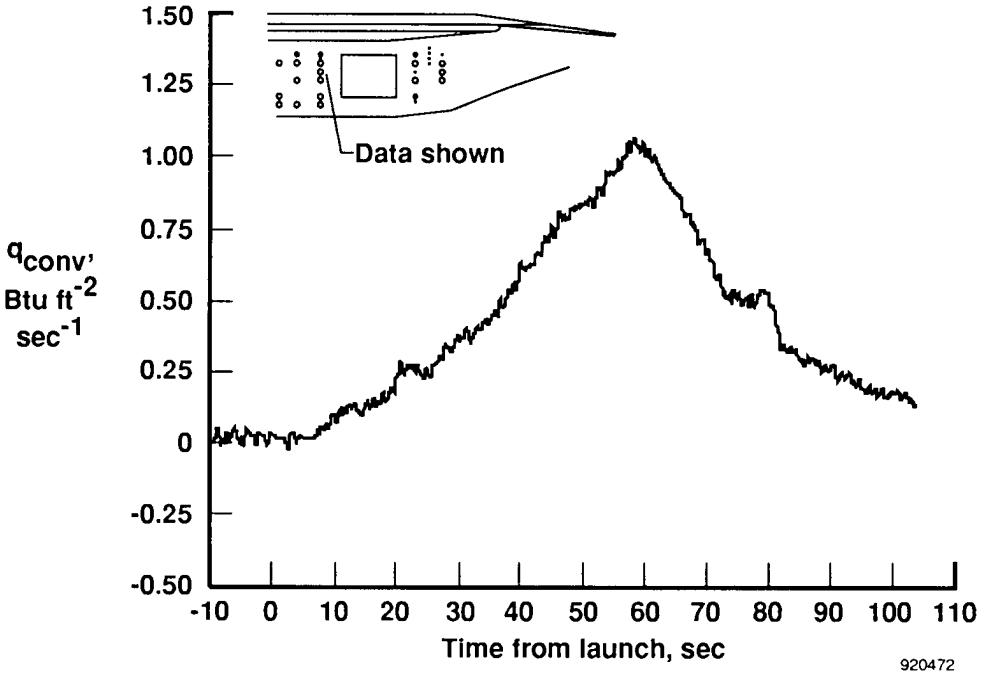

(d) FS = 253.1, z = 18.0.

Figure 11. Continued.

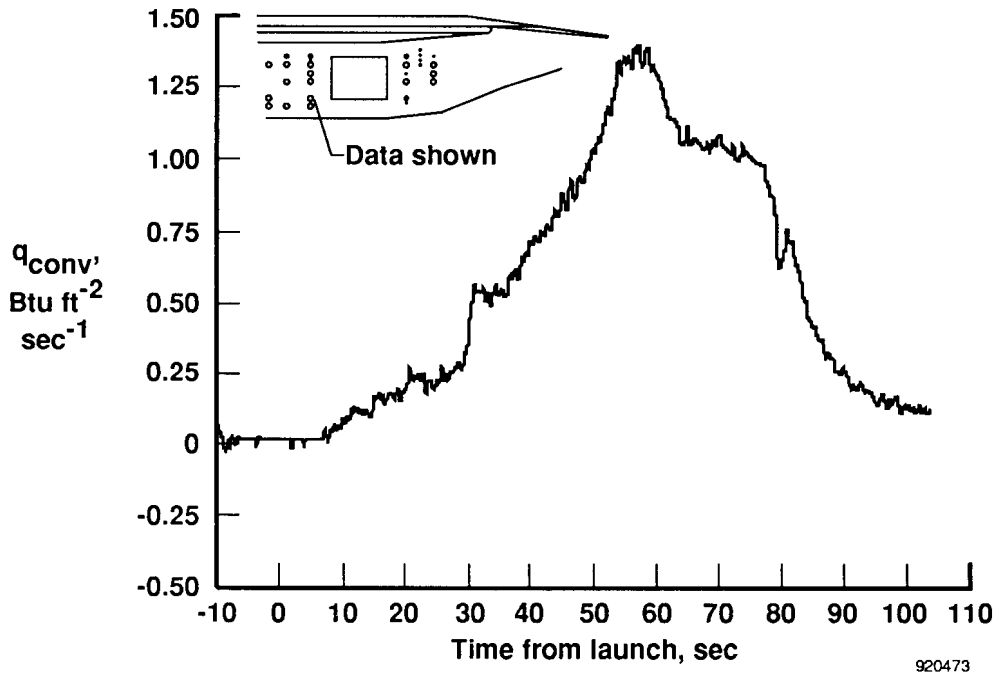

(e) FS = 253.1, z = 8.5.

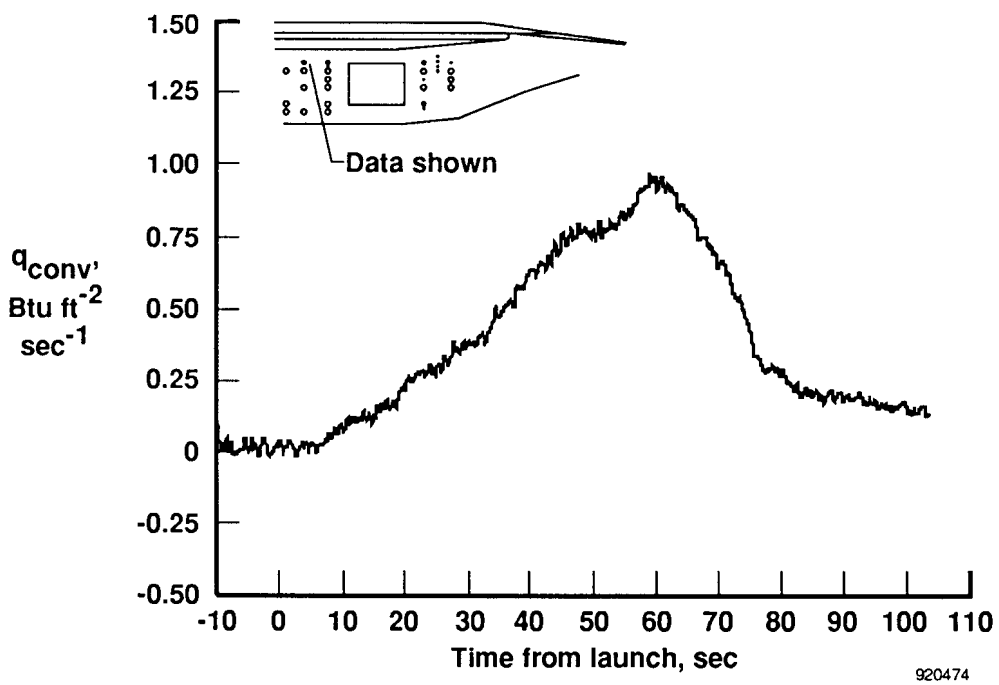

(f) FS = 246.2, z = 23.0.

Figure 11. Continued.

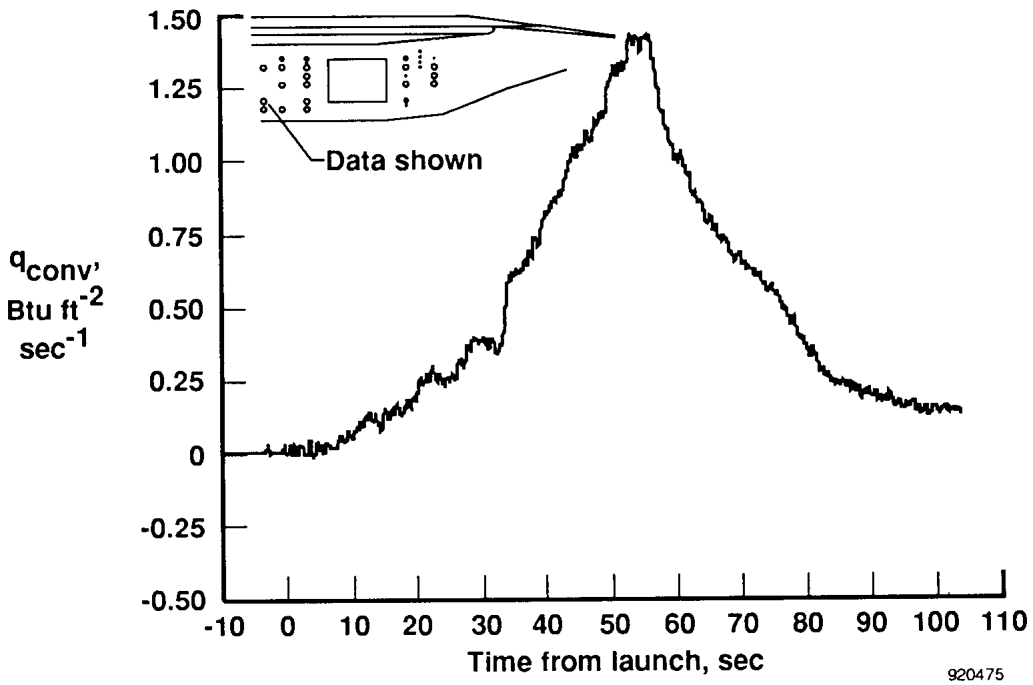

(g) FS = 241.0, z = 11.0.

Figure 11. Concluded.

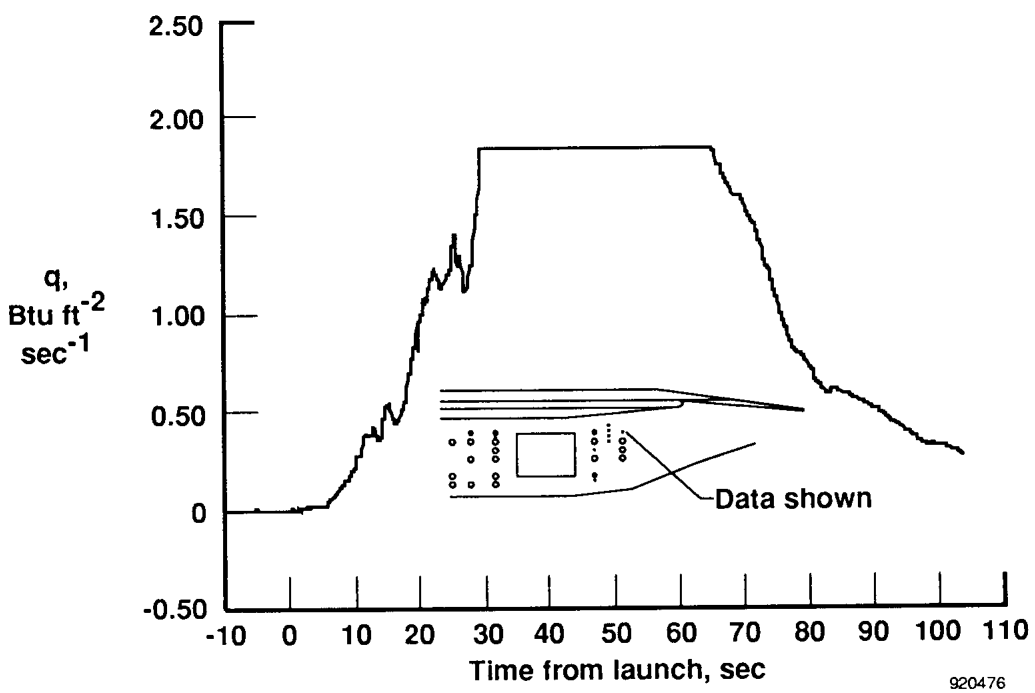

(a) FS = 288.4, z = 23.0.

Figure 12. Calorimeter heat-flux time histories.

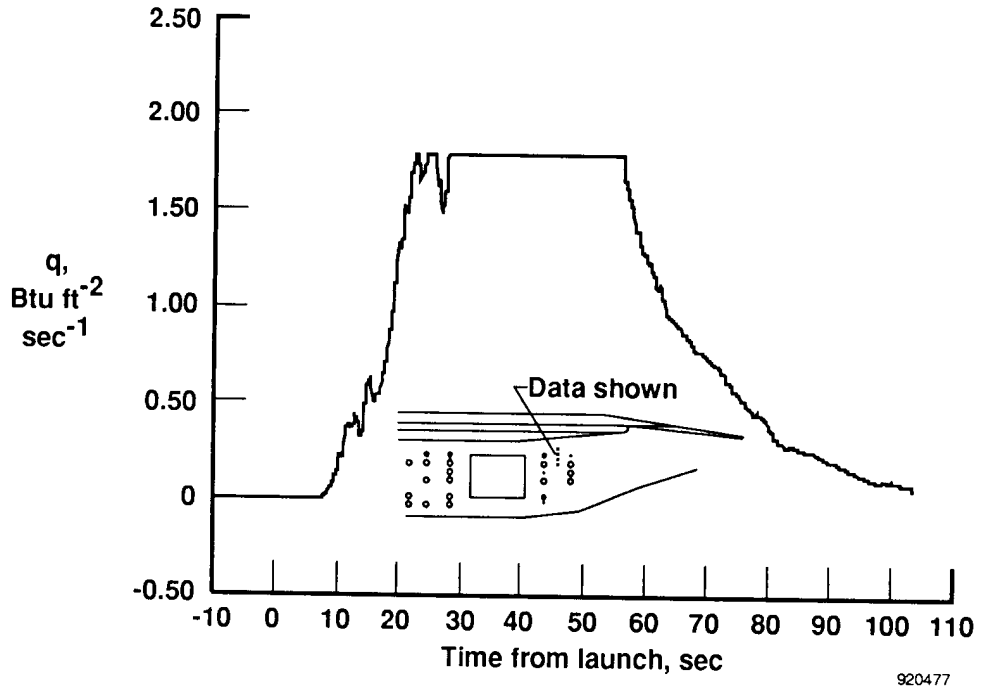

(b) FS = 284.5, z = 23.5.

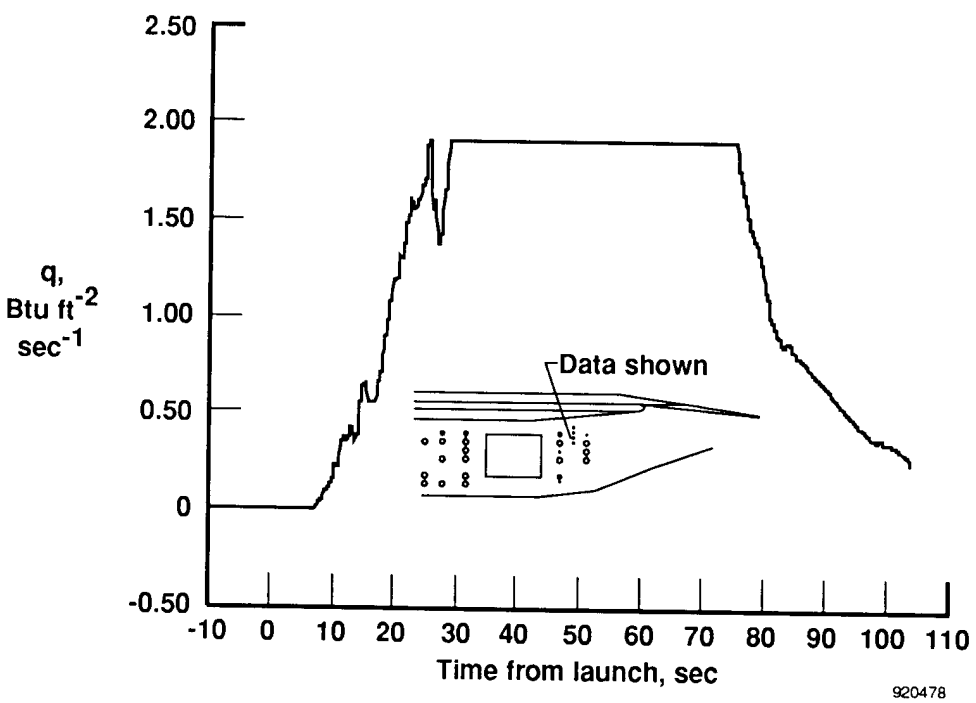

(c) FS = 284.5, z = 22.0.

Figure 12. Continued.

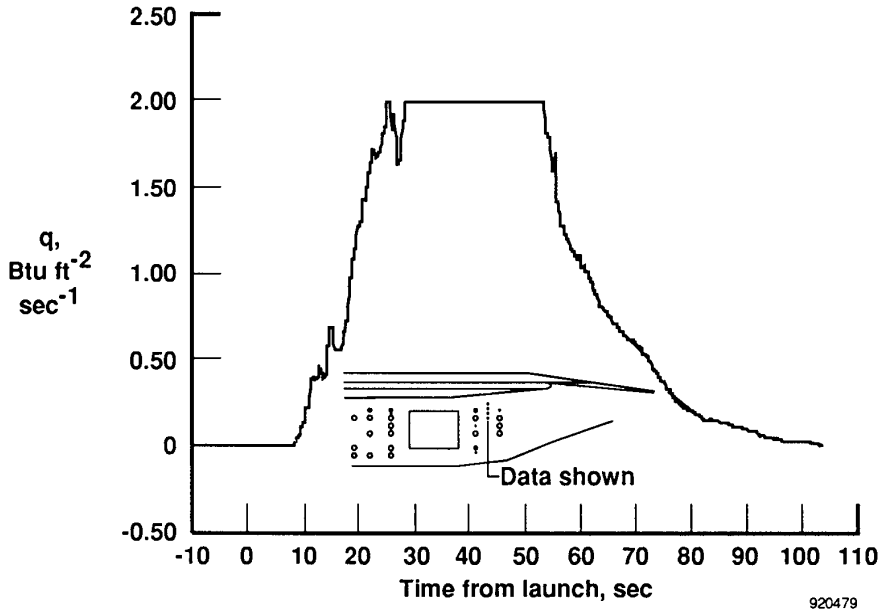

(d) FS = 284.5, z = 20.5.

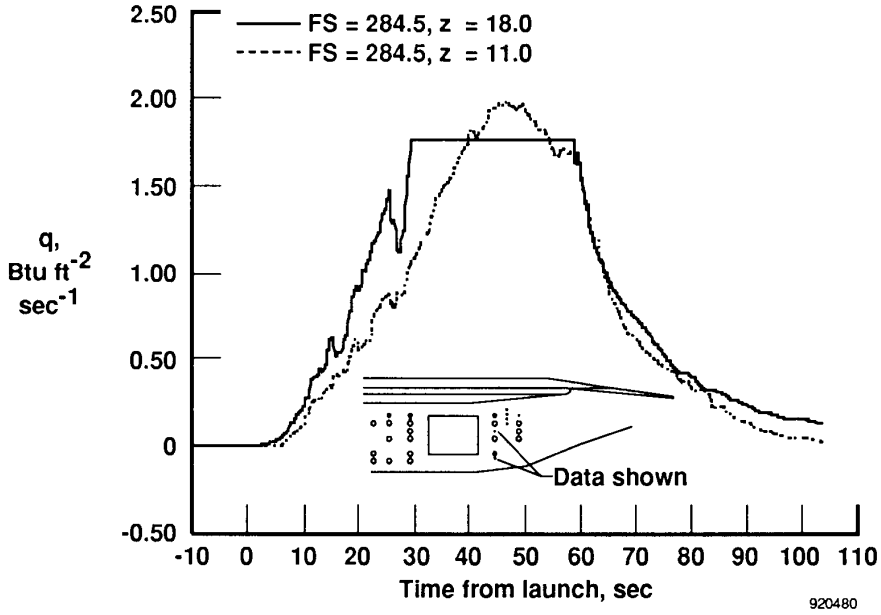

(e) FS = 284.5, z = 18.0 and FS = 284.5, z = 11.0.

Figure 12. Continued.

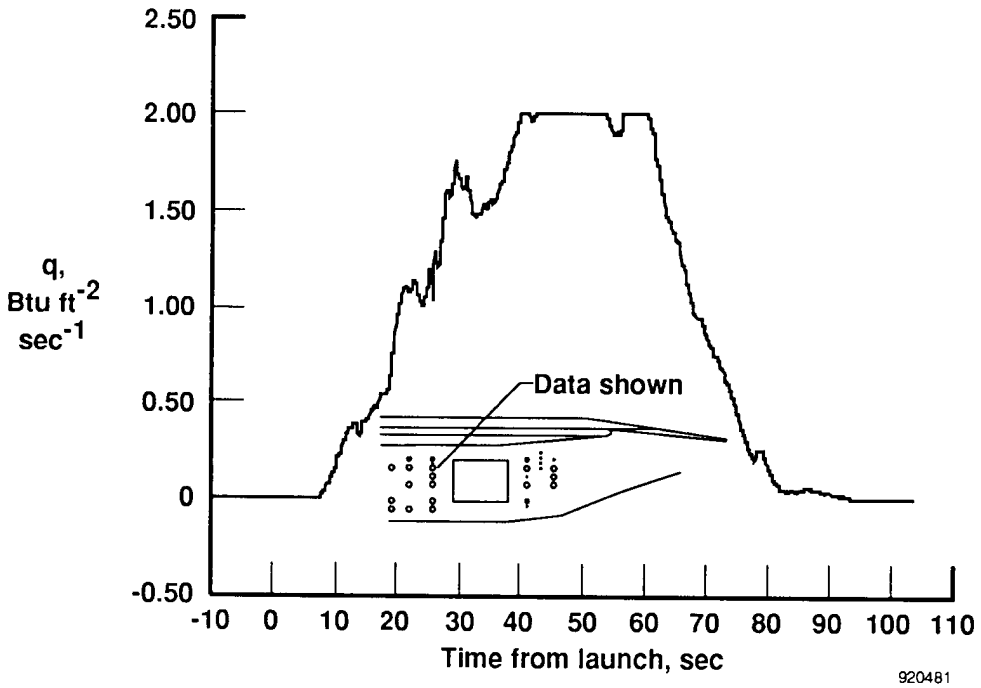

(f) FS = 253.1, z = 23.0.

Figure 12. Concluded.

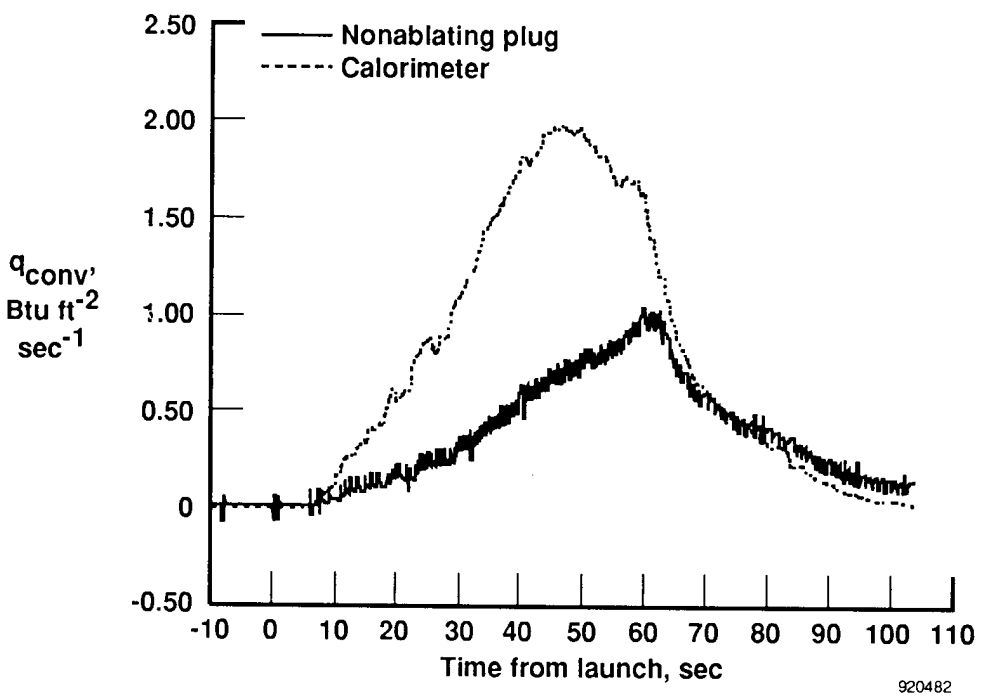

(a) FS = 280.6, z = 11.0.

Figure 13. Heat-flux time histories from collocated calorimeters and nonablating plugs.

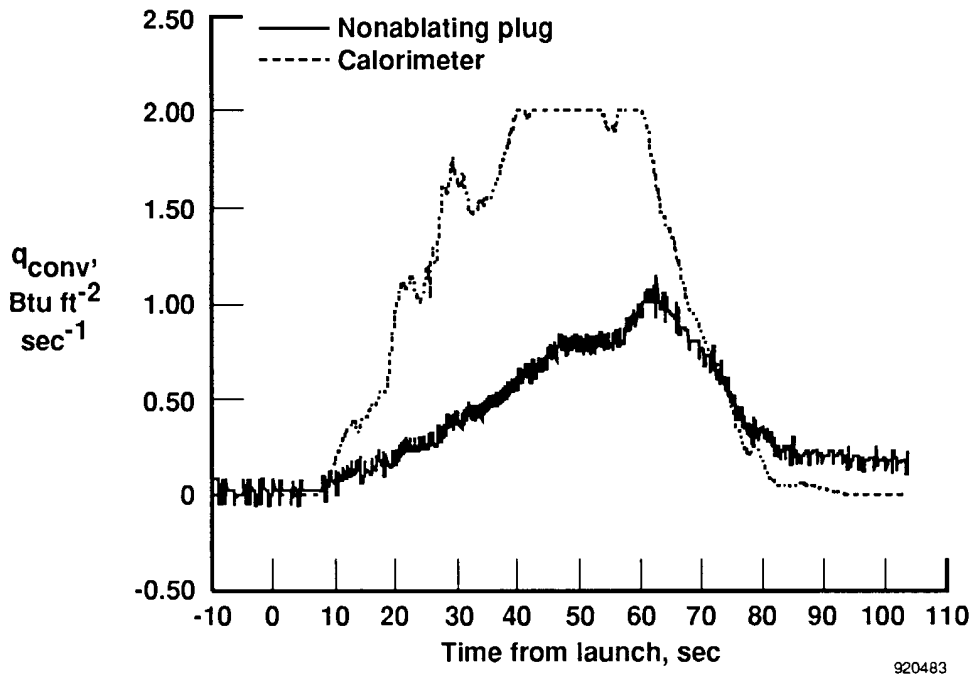

(b) FS = 253.1, z = 23.0.

Figure 13. Concluded.

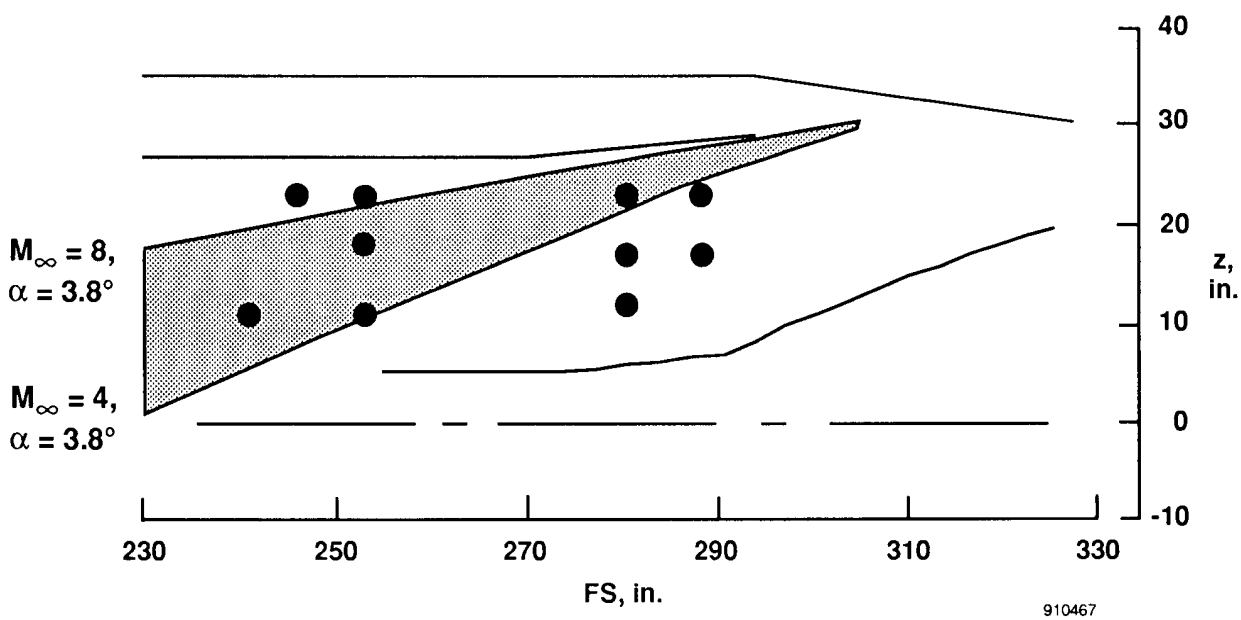

(a) Estimated wing leading-edge shock location, projected on fillet, from two-dimensional wedge theory.

Figure 14. Fillet sidewall reference heating for nonablating plugs.

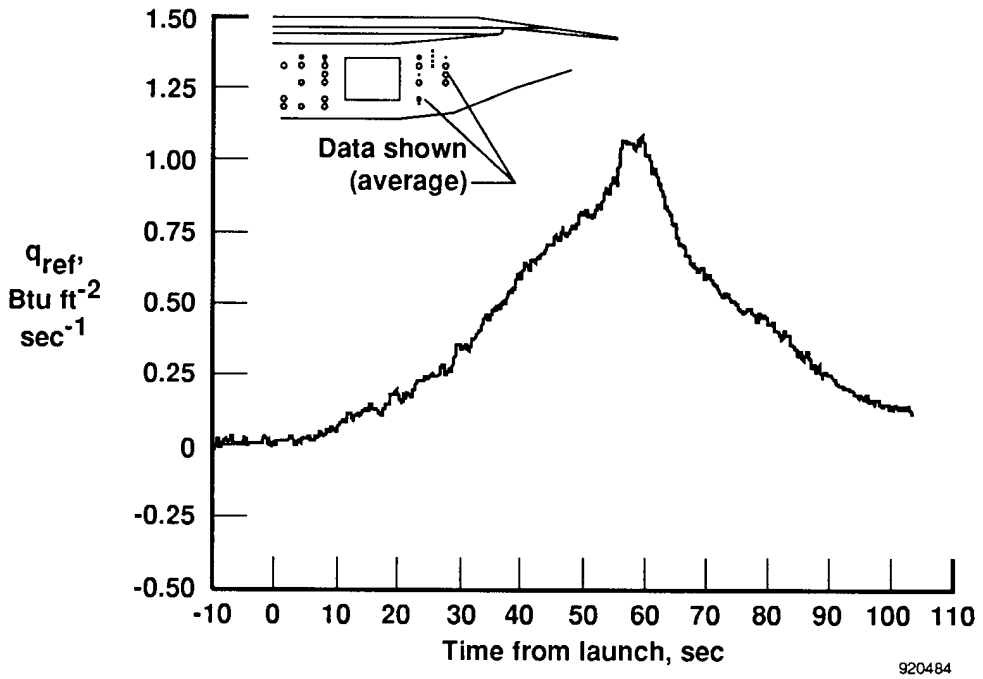

(b) Nonablating plug reference heating averaged from two plugs.

Figure 14. Concluded.

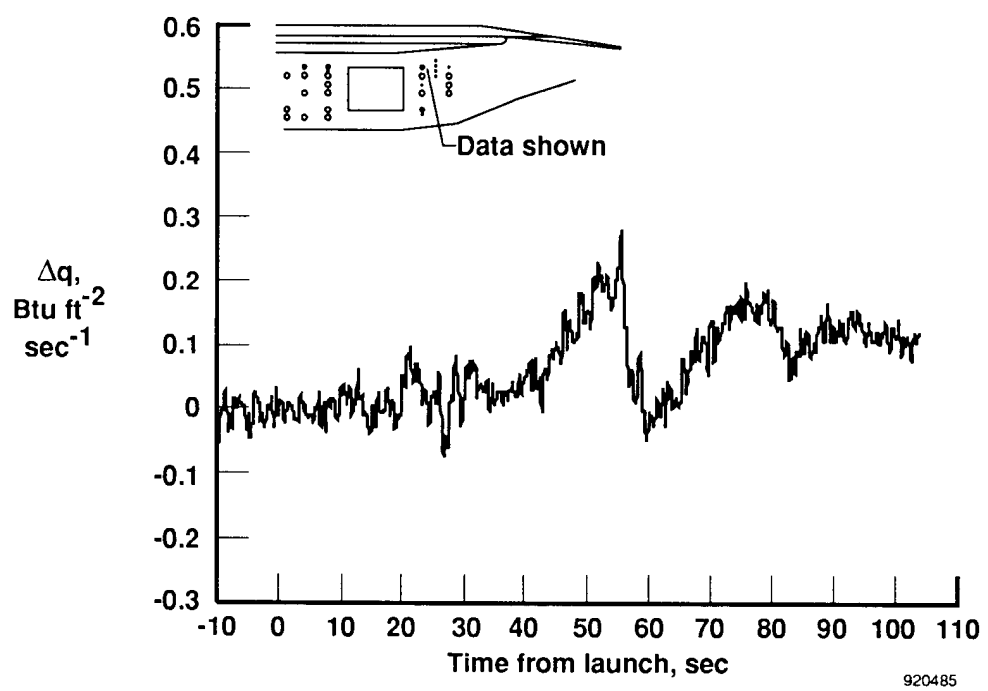

(a) FS = 280.6, z = 23.0.

Figure 15. Nonablating plug differential heating.

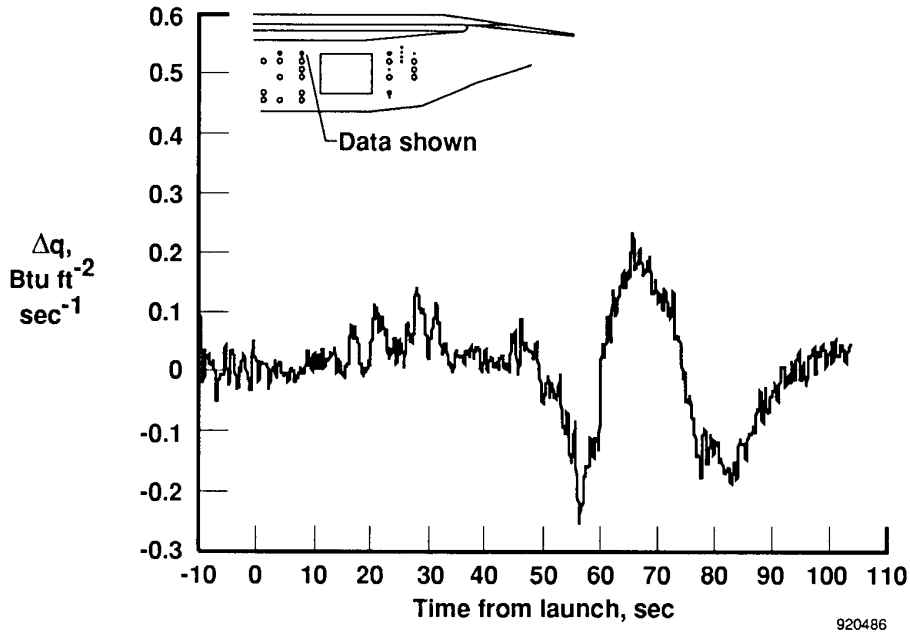

(b) FS = 253.1, z = 23.0.

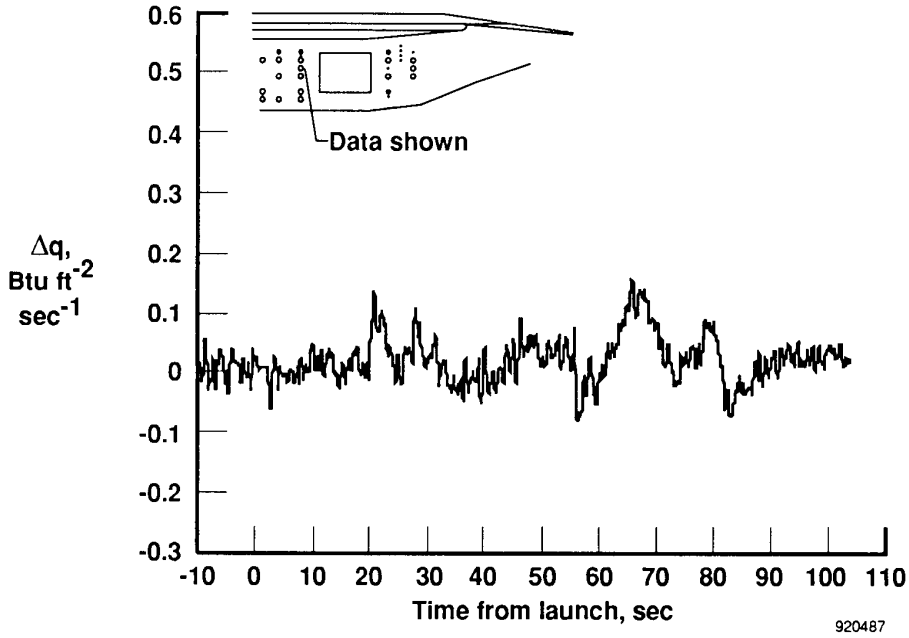

(c) FS = 253.1, z = 18.0.

Figure 15. Continued.

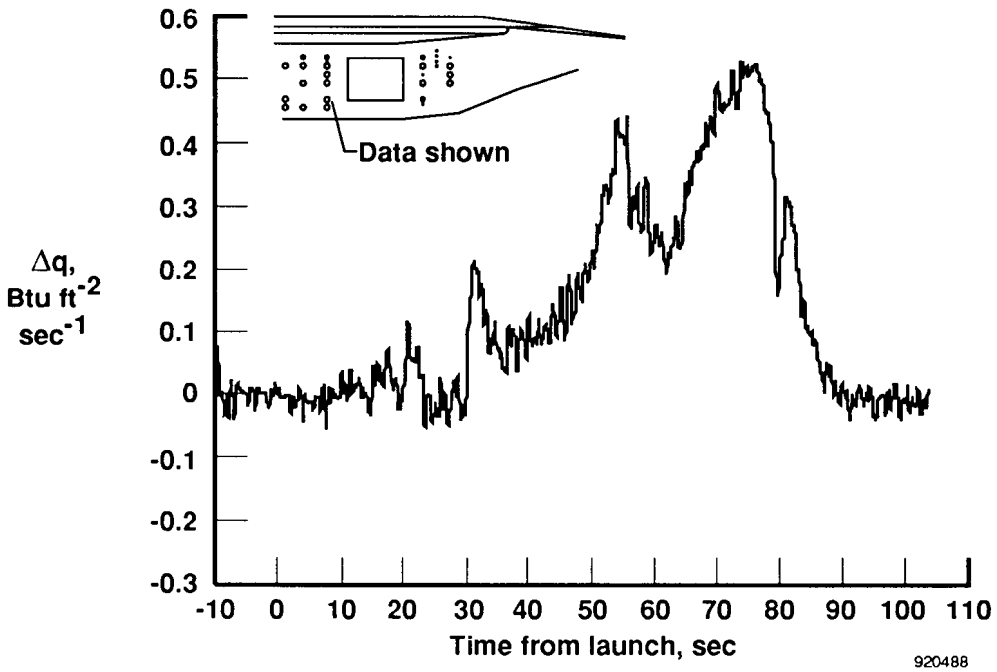

(d) FS = 253.1, z = 11.0.

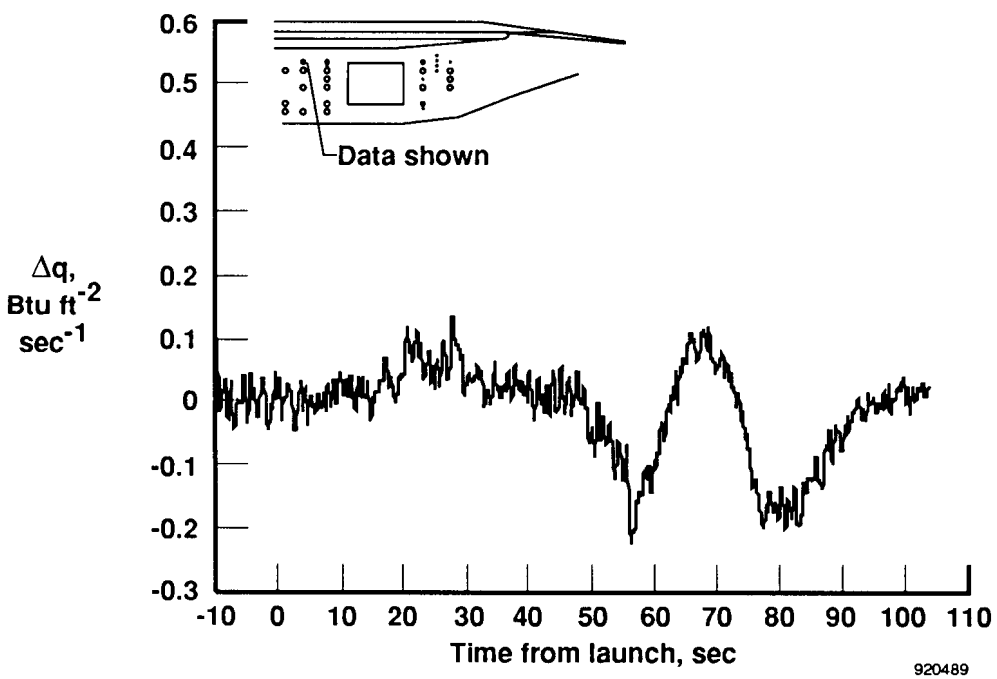

(e) FS = 246.2, z = 23.0.

Figure 15. Continued.

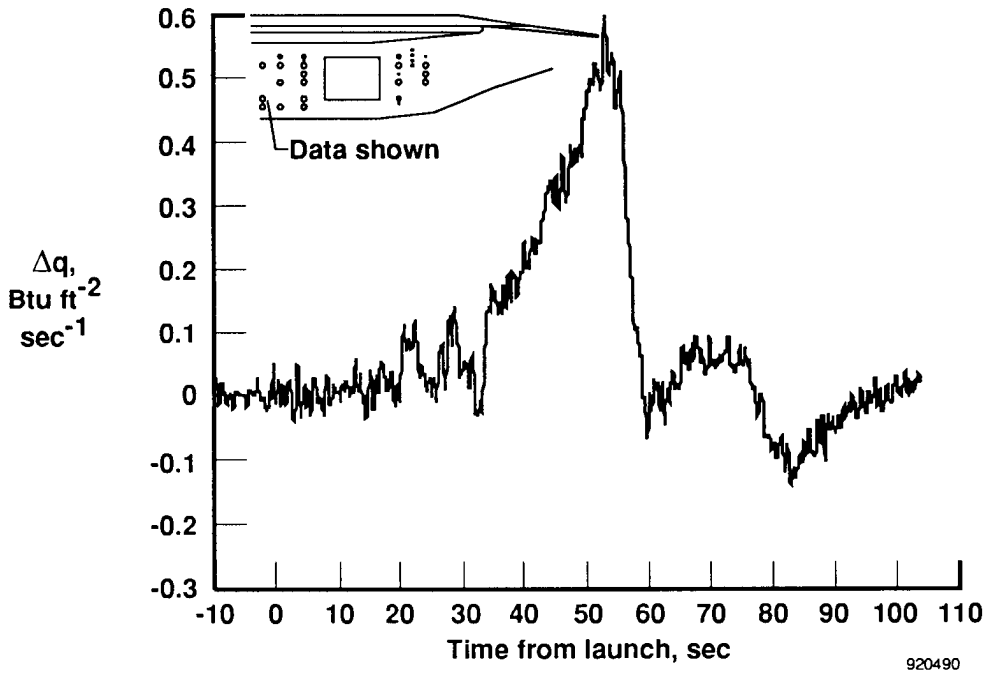

(f) FS = 241.0, z = 11.0.

Figure 15. Concluded.

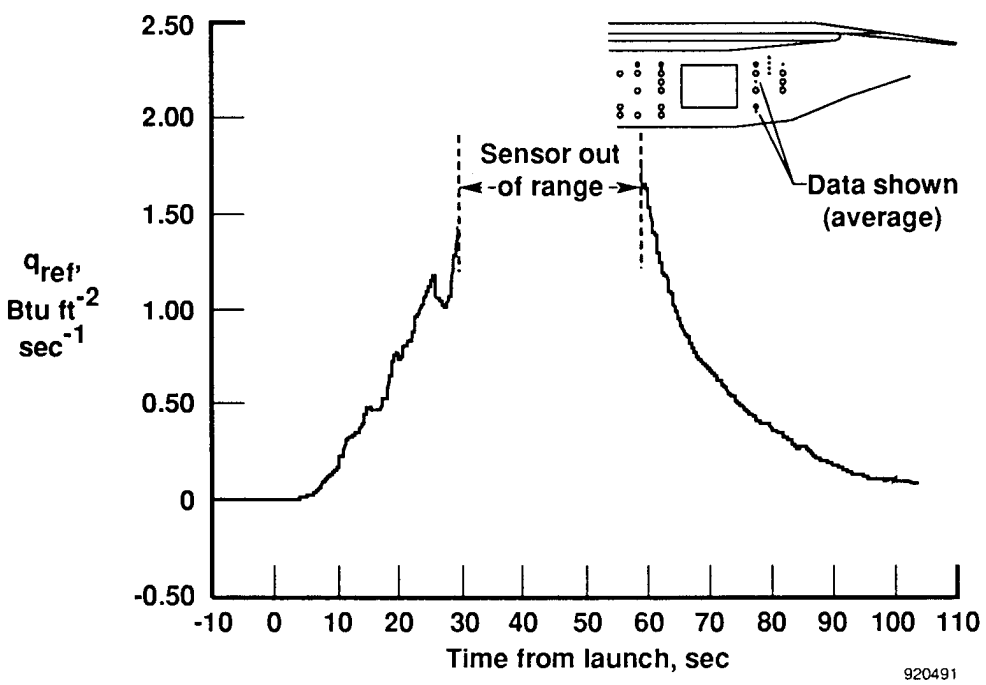

Figure 16. Colorimeter reference heating.

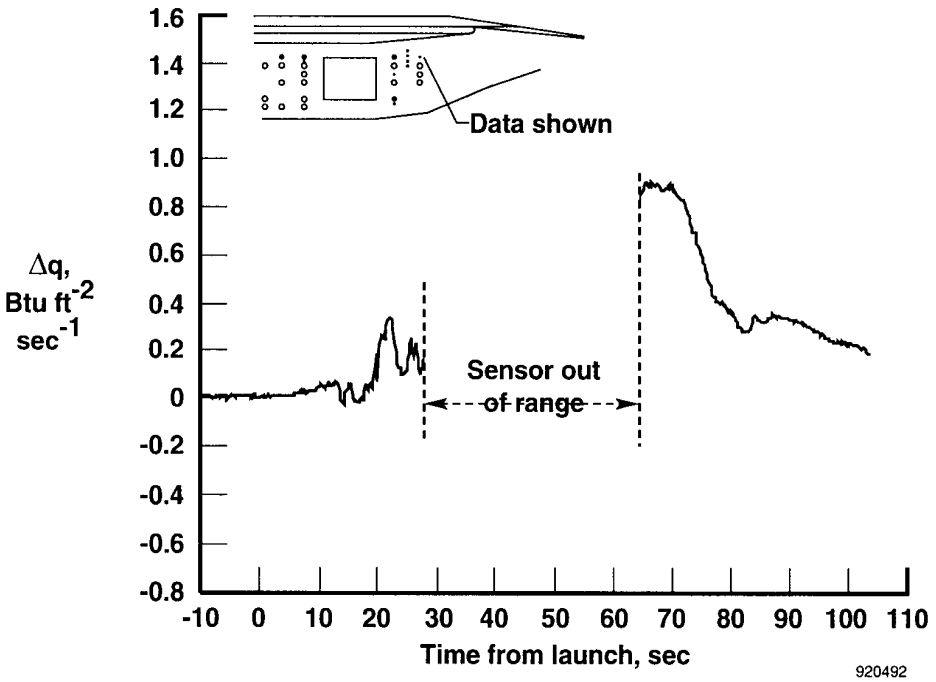

(a) FS = 288.4, z = 23.0.

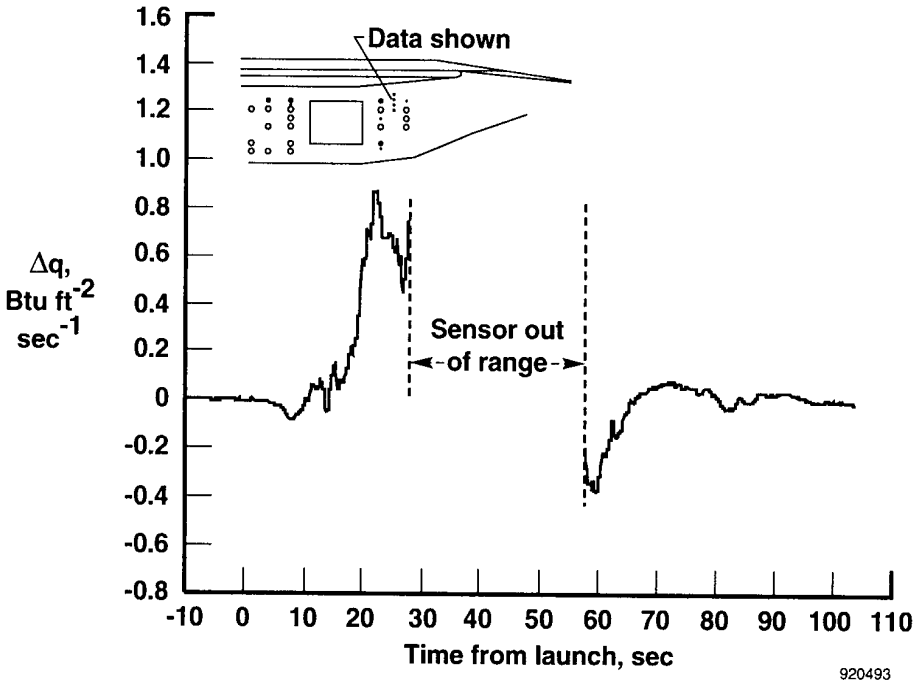

(b) FS = 284.5, z = 23.5.

Figure 17. Colorimeter differential heating.

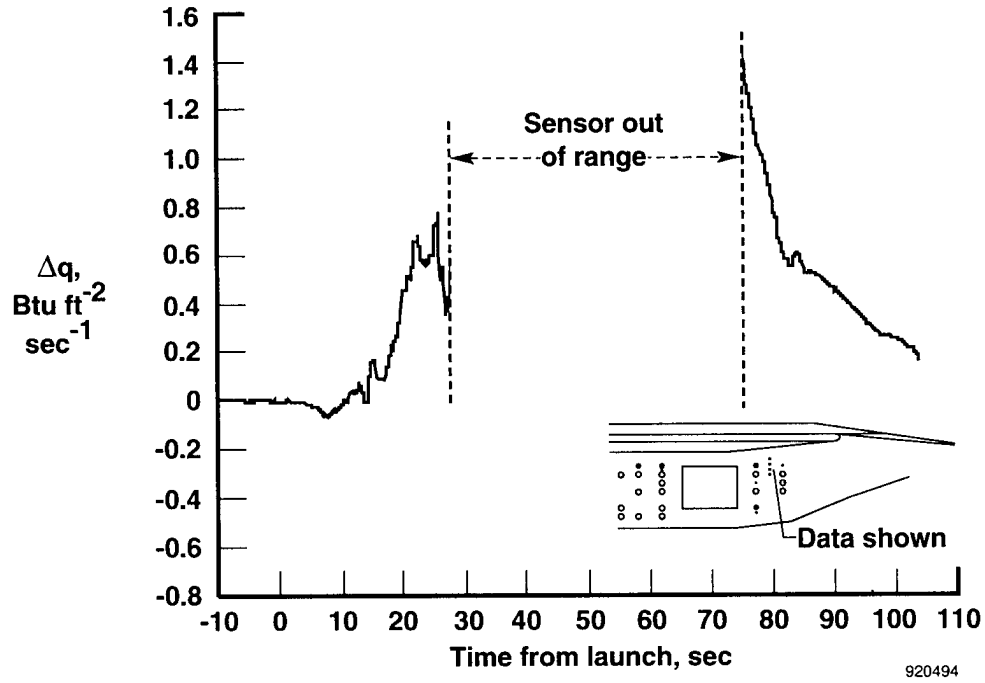

(c) FS = 284.5, z = 22.0.

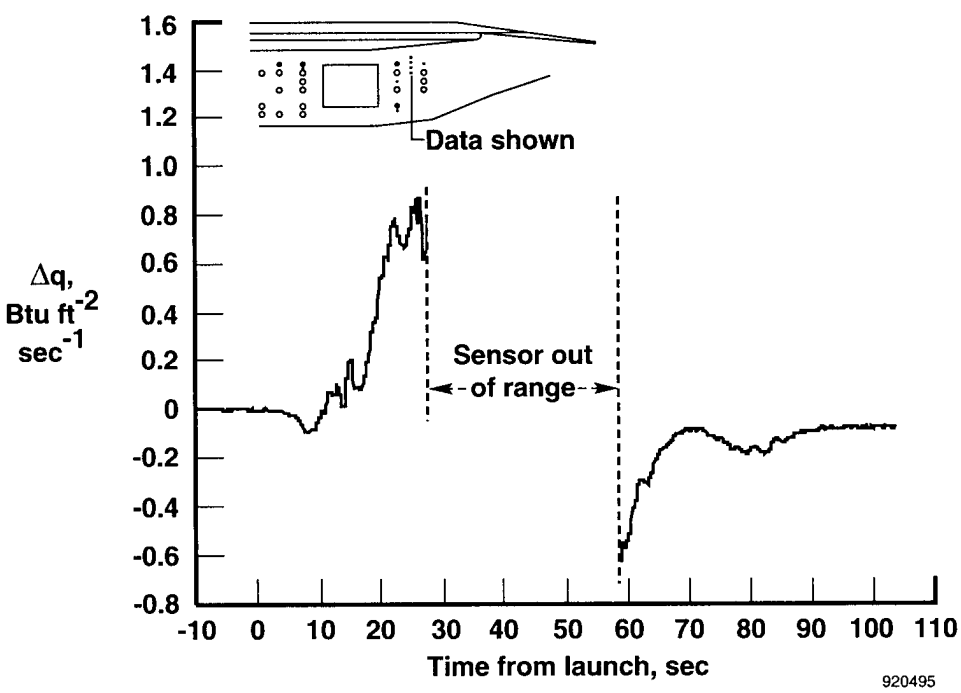

(d) FS = 284.5, z = 20.5.

Figure 17. Continued.

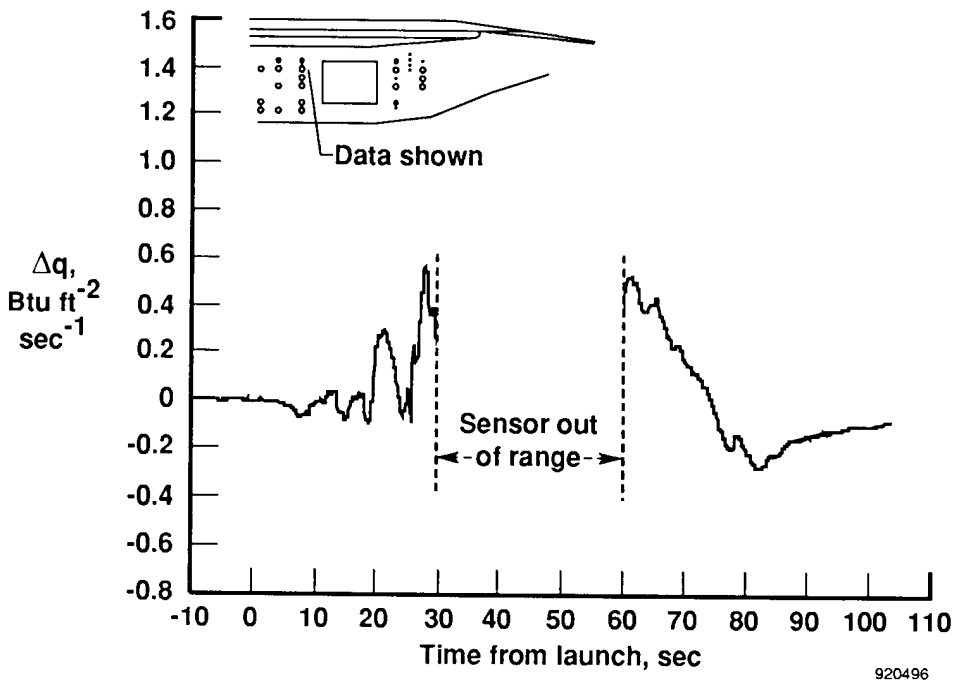

(e) FS = 253.1, z = 23.0.

Figure 17. Concluded.

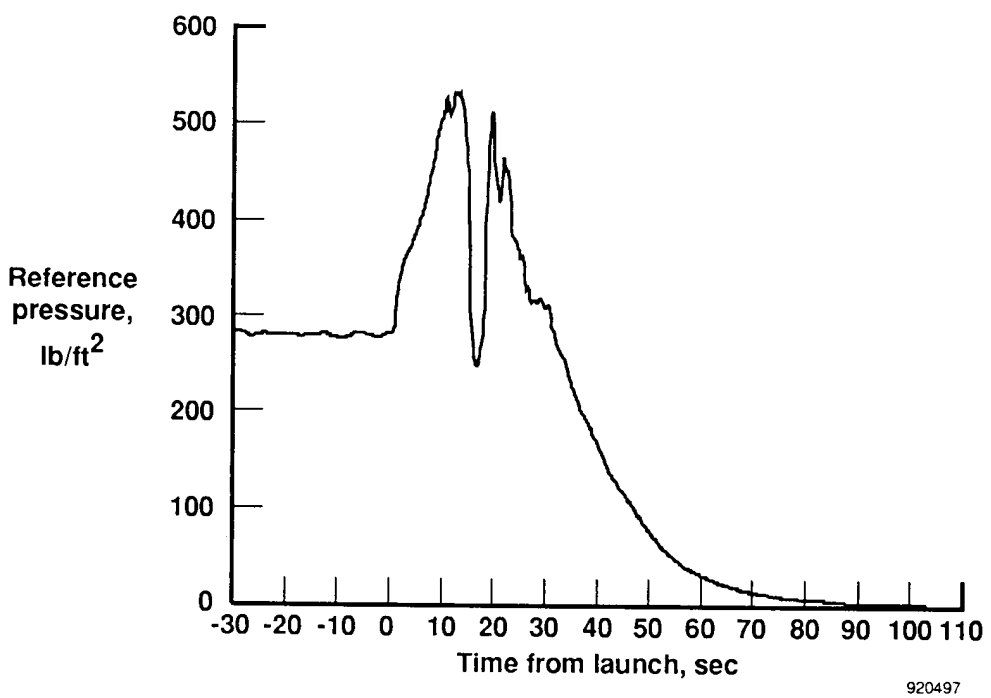

(a) Reference pressure.

Figure 18. Pressure-measurement time histories.

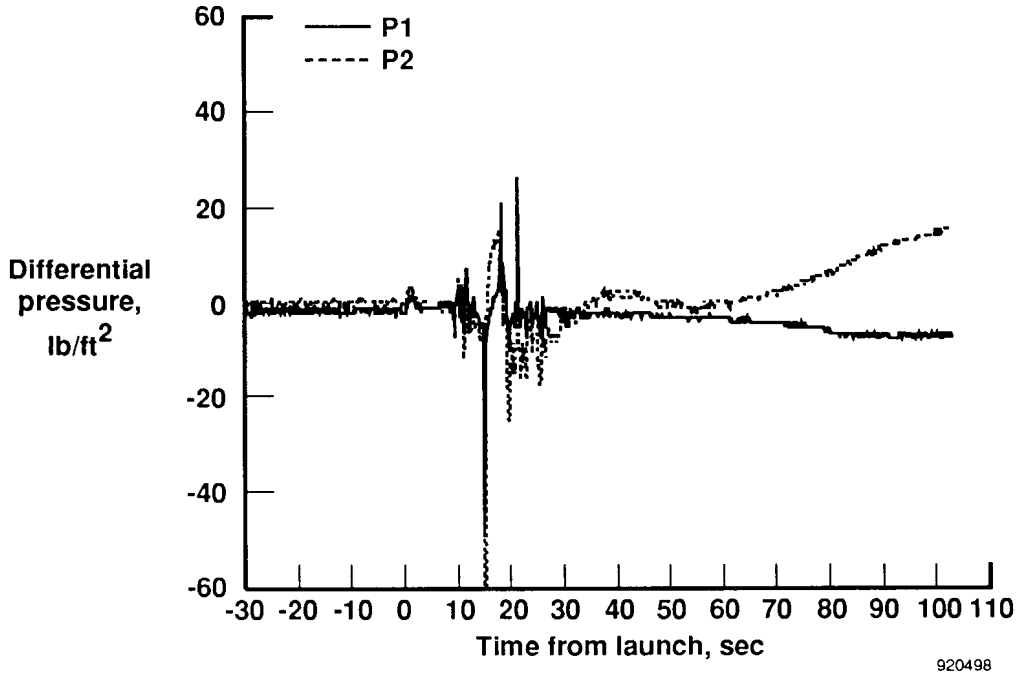

(b) Differential pressures for ports P1 and P2.

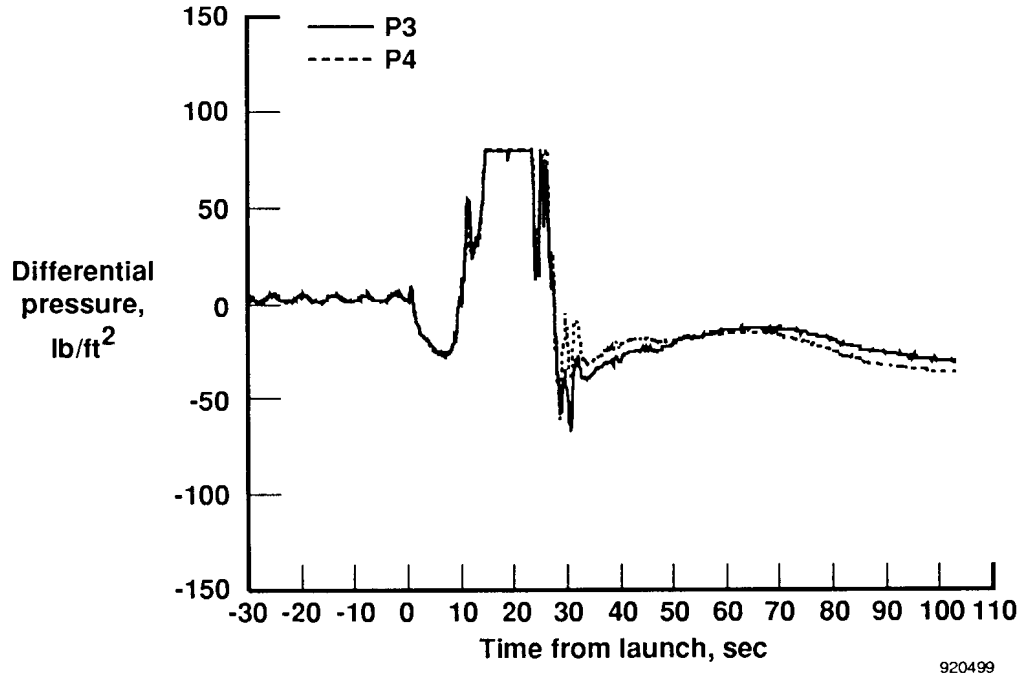

(c) Differential pressures for ports P3 and P4.

Figure 18. Continued.

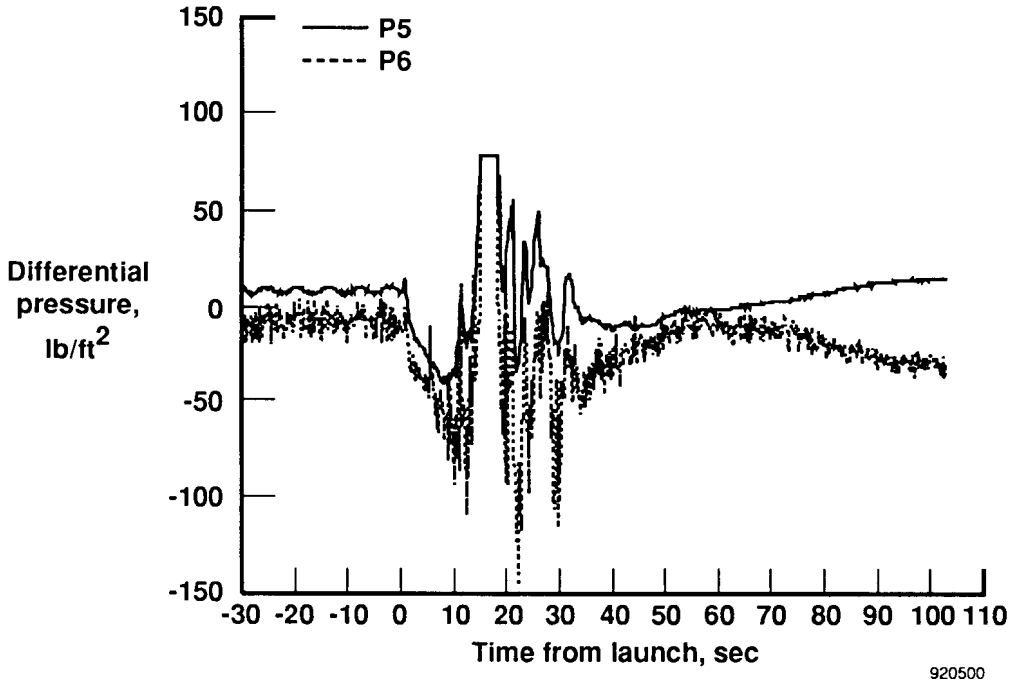

(d) Differential pressures for ports P5 and P6.

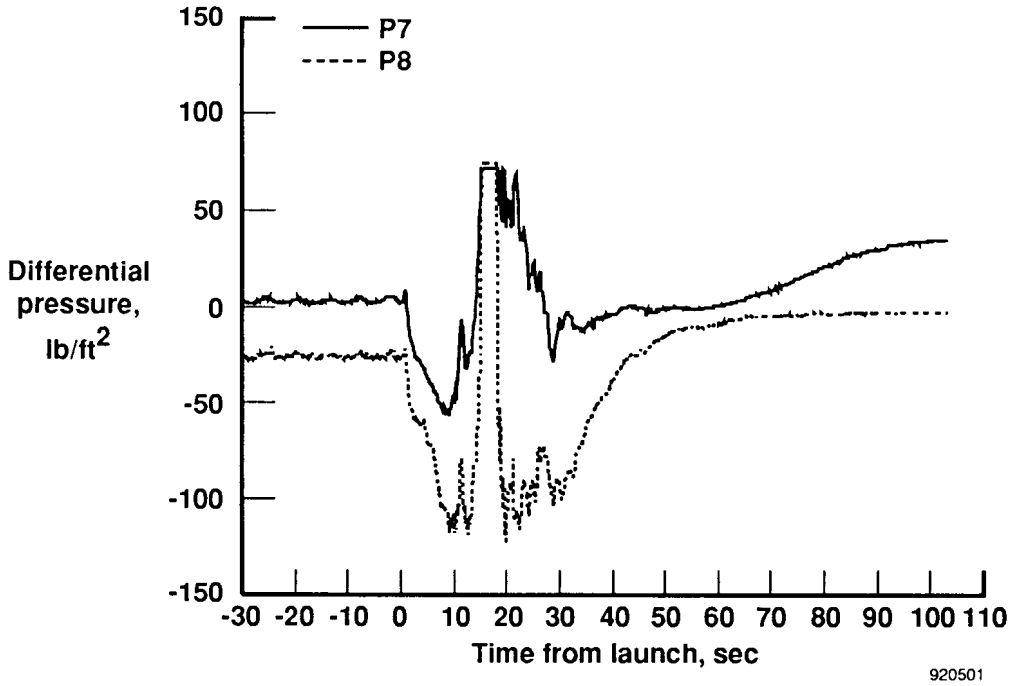

(e) Differential pressures for ports P7 and P8.

Figure 18. Concluded.

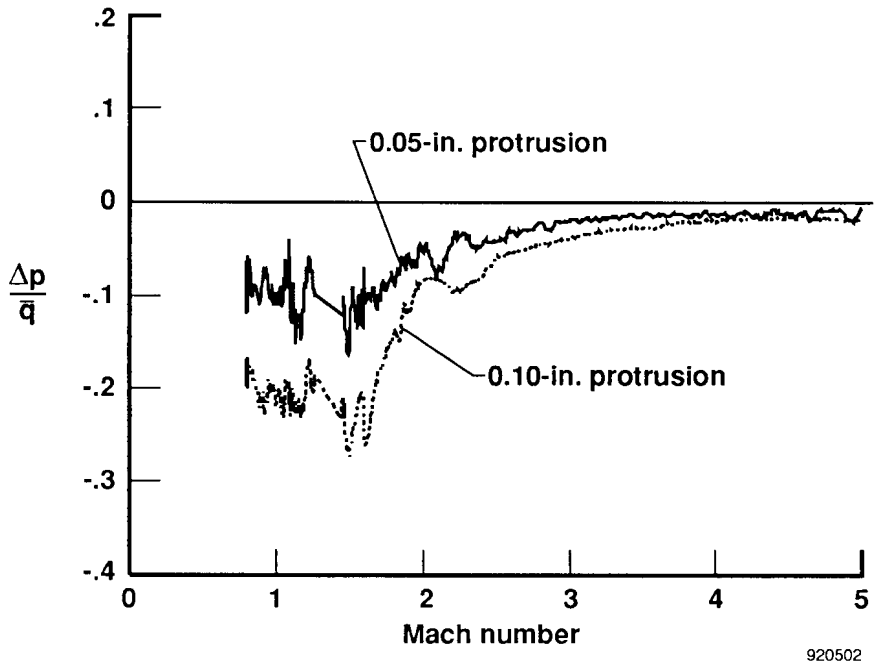

Figure 19. Effect of orifice protrusion on pressure measurement.

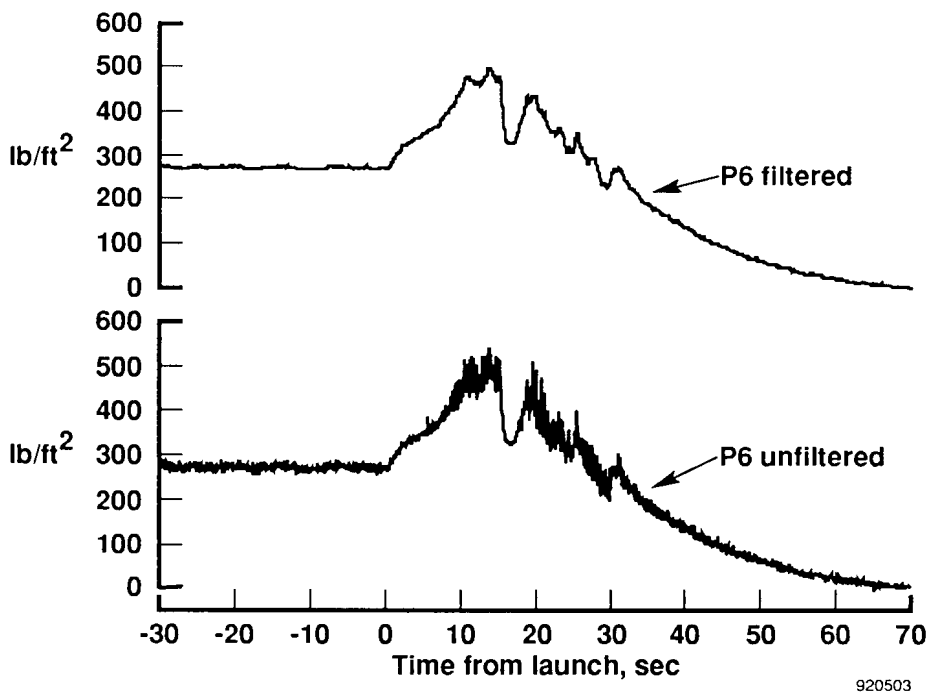

Figure 20. Comparison of filtered and unfiltered pressure measurement.

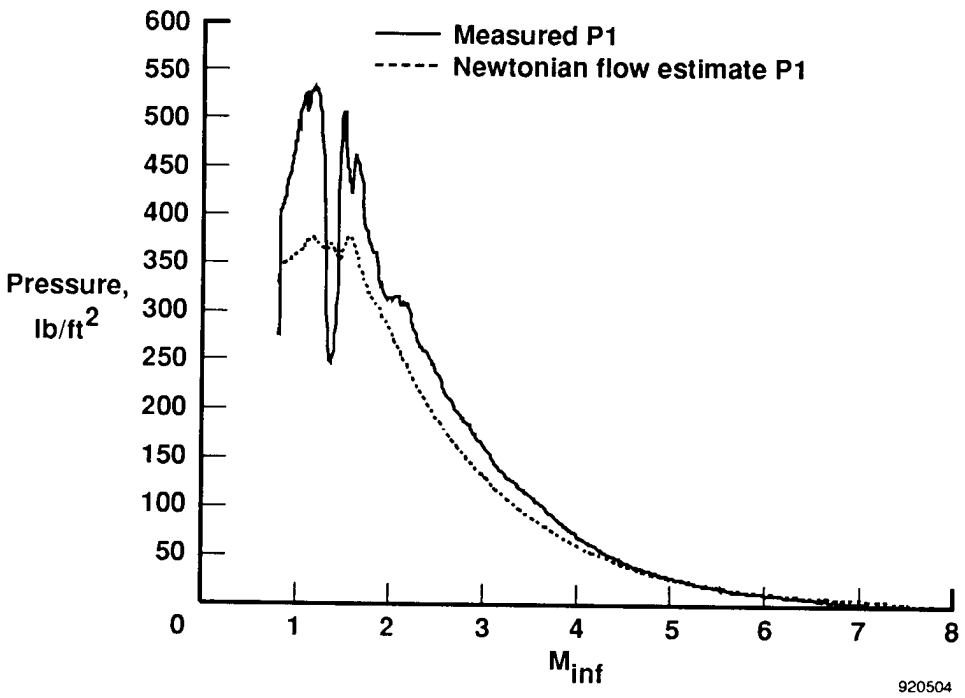

Figure 21. Comparison of a measured pressure with the modified-Newtonian flow estimate of pressure.

REPORT DOCUMENTATION PAGE

Form Approved
OMB No. 0704-0188

Public reporting burden for this collection of information is estimated to average 1 hour per response, including the time for reviewing instructions, searching existing data sources, gathering and maintaining the data needed, and completing and reviewing the collection of information. Send comments regarding this burden estimate or any other aspect of this collection of information, including suggestions for reducing this burden, to Washington Headquarters Services, Directorate for Information Operations and Reports, 1215 Jefferson Davis Highway, Suite 1204, Arlington, VA 22202-4302, and to the Office of Management and Budget, Paperwork Reduction Project (0704-0188), Washington, DC 20503.

1. AGENCY USE ONLY *(Leave blank)*	2. REPORT DATE	3. REPORT TYPE AND DATES COVERED
	October 1992	Technical Memorandum

4. TITLE AND SUBTITLE

Aerothermal Test Results From the Second Flight of the Pegasus® Booster

5. FUNDING NUMBERS

WU 505-59-40

6. AUTHOR(S)

Gregory K. Noffz, Timothy R. Moes, Edward A. Haering, Jr. (Dryden Flight Research Facility, Edwards, California); Paul Kolodziej (Ames Research Center, Moffett Field, California)

7. PERFORMING ORGANIZATION NAME(S) AND ADDRESS(ES)

NASA Dryden Flight Research Facility
P.O. Box 273
Edwards, CA 93523-0273

8. PERFORMING ORGANIZATION REPORT NUMBER

H-1827

9. SPONSORING/MONITORING AGENCY NAME(S) AND ADDRESS(ES)

National Aeronautics and Space Administration
Washington, DC 20546-0001

10. SPONSORING/MONITORING AGENCY REPORT NUMBER

NASA TM-4391

11. SUPPLEMENTARY NOTES

12a. DISTRIBUTION/AVAILABILITY STATEMENT

Unclassified — Unlimited
Subject Category 34

12b. DISTRIBUTION CODE

13. ABSTRACT *(Maximum 200 words)*

A survey of temperature, heat-flux, and pressure measurements was obtained at speeds through Mach 8.0 on the second flight of the Pegasus® air-launched space booster system. All sensors were distributed on the wing-body fairing or fillet. Sensors included thin foil-gauge thermocouples installed near the surface within the thermal protection system. Thermocouples were also installed on the surface of nonablating plugs. The resulting temperature time history allowed derivation of convective heat flux. In addition, commercially available calorimeters were installed on the fillet at selected locations. Calorimeters exhibited a larger change in measured heat flux than collocated nonablating plugs in response to particular events. Similar proportional variations in heat flux across different regions of the fillet were detected by both the calorimeters and nonablating plugs. Pressure ports were installed on some nonablating plugs to explore the effects of port protrusion and high-frequency noise on pressure measurements. The effect of port protrusion on static-pressure measurements was found to decrease with increasing Mach number. High-frequency noise suppression was found to be desirable but not required on any future flight.

®Pegasus is a registered trademark of Orbital Sciences Corp., Fairfax, Virginia.

14. SUBJECT TERMS

Aerothermal test results; Flight tests; Heat flux; Pegasus; Thermal protection

15. NUMBER OF PAGES

44

16. PRICE CODE

A03

17. SECURITY CLASSIFICATION OF REPORT	18. SECURITY CLASSIFICATION OF THIS PAGE	19. SECURITY CLASSIFICATION OF ABSTRACT	20. LIMITATION OF ABSTRACT
Unclassified	Unclassified	Unclassified	Unlimited

NSN 7540-01-280-5500

Standard Form 298 (Rev. 2-89)
Prescribed by ANSI Std. Z39-18
298-102

NASA-Langley, 1992